A&A 530, A33 (2011)
DOI: 10.1051/0004-6361/201016330
© ESO 2011

Astronomy & Astrophysics

Silicon depletion in damped Ly α systems

The S/Zn method⋆,⋆⋆

G. Vladilo[1], C. Abate[3,2], J. Yin[4,2], G. Cescutti[2], and F. Matteucci[2]

[1] Osservatorio Astronomico di Trieste, Istituto Nazionale di Astrofisica, via G.B. Tiepolo 11, Trieste, Italy
e-mail: vladilo@oats.inaf.it
[2] Dipartimento di Fisica, Sezione di Astronomia, Università di Trieste, via G.B. Tiepolo 11, Trieste, Italy
[3] Astronomical Institute Utrecht, Buys Ballot Lab, 3508 TA Utrecht, The Netherlands
[4] Shanghai Astronomical Observatory, 80 Nandan Road, Shanghai 200030, PR China

Received 15 December 2010 / Accepted 11 March 2011

ABSTRACT

Silicates are an important component of interstellar dust that has been poorly investigated in high redshift galaxies. As a preliminary step to studying silicates at high redshift, we survey silicon depletions in damped Ly α (DLA) systems. Silicon depletion is mild in the Galactic interstellar medium (ISM) and is expected to be weaker in most DLA systems, so we introduce a method for improving the accuracy of DLA depletion measurements. We compare abundance ratios measured in the gas with calculations of total abundance ratios of gas and dust predicted by models of galactic chemical evolution tailored for DLA systems. To tune the model parameters, we use the dust-free observational diagram S/Zn versus Zn/H, and we also compare the look back time estimated from the absorption redshift with the evolutionary time predicted by the model. By applying our method to a large set of DLA column densities, we succeeded in measuring the depletion of silicon in 74 systems. For comparison, we also measure iron and magnesium depletions (105 and 10 systems, respectively) with the same method. The mean depletion of silicon that we derive, $\langle\delta_{\rm Si}\rangle \simeq -0.27 \pm 0.16$ dex, is surprisingly close to that of iron, $\langle\delta_{\rm Fe}\rangle \simeq -0.42 \pm 0.28$ dex, despite iron being much more depleted than silicon in the Galactic ISM. Silicon depletion in DLA systems does not correlate with metallicity, at variance with iron depletion, for which we confirm a rise with [Fe/H] found in previous work. Magnesium depletion seems to behave more in accordance with silicon than with iron. The different behaviors of the silicon and iron depletions suggests a complex history of dust production at the early stages of galactic chemical evolution.

Key words. ISM: abundances – dust, extinction – galaxies: high-redshift – quasars: absorption lines – methods: miscellaneous – instrumentation: spectrographs

1. Introduction

Interstellar dust plays a key role in a variety of physical and chemical processes relevant to galactic evolution. The presence of dust affects the observed spectral energy distribution of astronomical sources and diffuse extragalactic backgrounds. Characterizing the properties of dust at high redshift, even if challenging, is an important step to improve our understanding of the early Universe. In particular, models of dust production and evolution in galaxies (e.g. Dwek 1998; Calura et al. 2008; Zhukovska et al. 2008) would greatly benefit from new observational constraints on the dust properties at early stages of chemical evolution.

Quasar spectroscopy is an excellent tool for probing the dust at high-redshift: the quasar absorption line systems with neutral hydrogen column density[1] $N(\mathrm{H\,I}) \gtrsim 10^{20.3}$ atoms cm^{-2}, known as *damped Ly α (DLA) systems*, originate in the interstellar medium of foreground galaxies (Wolfe et al. 1986, 2005) and probe the dust embedded therein.

Evidence of dust in individual DLA systems has been found as a result of searches for classical dust indicators, such as the 217.5 nm extinction "bump" (Junkkarinen et al. 2004; Wang et al. 2004; Srianand et al. 2008a), the 9.7 μm silicate absorption (Kulkarni et al. 2007, 2011), and the quasar reddening due to foreground absorption (Vladilo et al. 2006; Jiang et al. 2010). The DLA systems investigated in these studies offer unique opportunities for characterizing the dust in distant galaxies. However, these dust-rich absorbers are the exception rather than the rule: the bulk of the DLA population is believed to be dust-poor. Evidence of this comes from the extremely weak signal of mean reddening in quasar samples with intervening absorbers (Murphy & Liske 2004; Vladilo et al. 2008; Frank & Peroux 2010) and from studies of radio-selected quasar samples unbiased by dust extinction (Ellison et al. 2001; Jorgenson et al. 2006). The low level of dust is broadly consistent with the low level of metal enrichment of DLA systems (Pettini et al. 1994).

In this work, we are interested in characterizing the properties of dust in the metal-poor population of DLA systems to improve our understanding of the early build-up and chemical evolution of dust in galaxies. In particular, we wish to trace the presence of silicon in dust, as a preliminary step for studies of silicates at high redshift. Silicates are a widespread component

⋆ Tables 4–7 and part of Table 8 are available in electronic form at http://www.aanda.org

⋆⋆ Full Table 8 is only available at the CDS via anonymous ftp to cdsarc.u-strasbg.fr (130.79.128.5) or via http://cdsarc.u-strasbg.fr/viz-bin/qcat?J/A+A/530/A33

[1] The column density is the number of atoms or ions of interest in a column of unit area along the line of sight to the background source (quasar or star).

of interstellar dust, representing up to ∼70% of the core mass of dust grains (Draine 2003; Henning 2010). The first detections of silicate absorption at 9.7 μm in dust-rich DLA systems at low redshift (Kulkarni et al. 2007, 2010) indicate that times are ripe for understanding whether or not silicates are pervasive in the bulk of the DLA population at $z_{\rm abs} \gtrsim 2$.

To accomplish our goal, we rely on an observational technique that is effective in finding the signature of dust even in metal-poor systems, i.e. the study of abundance ratios of elements with different affinities with dust. Chemical abundances of DLA systems can be obtained with high accuracy from the analysis of optical/UV absorption lines. Atoms locked into dust grains do not contribute to the optical/UV absorption-line cross-section[2] and are not counted in the column density determinations. For this reason, the abundances of *refractory* elements, which tend to stay in the dust, appear to be *depleted* relative to the abundances of *volatile* elements, which tend to stay instead in the gas. Therefore measuring the abundance ratios of volatile and refractory elements allows us to probe the dust in DLA systems.

The first application of this technique to DLA systems was based on the Zn/Cr ratio (Pettini et al. 1994, 1997). The apparent overabundance of the Zn/Cr ratio in DLA systems is similar to that found in the Galactic ISM, where we know that zinc is volatile while chromium is refractory. Starting from this study, it became clear that it is unsafe to trace the metallicity[3] of DLA systems using refractory elements, such as iron. For this reason, zinc has become the first choice in studies of DLA metallicity, yielding a typical value [Zn/H] $\simeq -1.1$ dex (Pettini et al. 1994; Akerman et al. 2005), with a large dispersion at each redshift and a gradual rise with cosmic time (e.g. Vladilo et al. 2000; Prochaska et al. 2001).

Zinc has also become the reference element for estimating the differential depletion of refractory elements, using abundance ratios such as Zn/Fe or Zn/Cr. To measure the absolute depletion of the refractory element from the observed ratios, we need to know in advance the intrinsic total ratios (gas plus dust) and also to take into account that zinc can be slightly depleted. By adopting a solar, or slightly supersolar, intrinsic Zn/Fe ratio, as observed in Galactic metal-poor stars, and by modeling zinc depletion using Galactic ISM observations, in a previous work we were able to measure iron depletions in 38 DLA systems (Vladilo 2004). In this way we found evidence for a rise of iron depletion with metallicity. This rise disagrees with the expectations, based on studies of the local Universe, that the dust-to-metal ratio should be roughly constant in the course of chemical evolution.

In the present work, we wish to study the depletion of silicon. Measuring silicon depletion in metal-poor galaxies is rather challenging because silicon is less depleted than iron and is expected to be hardly depleted at all in metal-poor gas. This probably explains why searches for silicon depletion in the Small Magellanic Cloud (SMC) have provided contrasting results (Welty et al. 2001; Sofia et al. 2006). In DLA systems, Si depletion has only been estimated in a few dust-rich molecular absorbers (Noterdaeme et al. 2007; Jiang et al. 2010). More often, the very existence of silicon depletion has not been considered, to the point of treating silicon as a dust-free metallicity indicator in the absence of abundances of volatile elements.

The challenge of measuring silicon depletion in DLA systems must be confronted with new tools. Here we propose a method specifically developed for this purpose that has two main novelties relative to previous work. The first is that we use sulfur, in conjunction with zinc, to define a pair of volatile elements to be used as a dust-free reference for abundances. The second is that we use models of galactic chemical evolution designed for DLA systems to estimate the total abundance ratios (gas plus dust) used to derive the depletions. In practice, we use the S/Zn ratio as a dust-free diagnostic of chemical evolution to constrain the chemical history of DLA systems. This work has been possible thanks to the continuous accumulation of new S II column density measurements in DLA systems, starting from the first work designed to study the S/Zn ratio as a dust-free indicator of chemical evolution of DLA host galaxies (Centurión et al. 2000).

Our adopted method is described in the next section. The observational database, which includes a few new measurements of S II column densities, is presented in Sect. 3. The models of galactic chemical evolution for DLA systems are discussed in Sect. 4. The depletions are presented in Sect. 5 and discussed in Sect. 6.

2. The method

2.1. Assumptions

The abundance ratios that we measure in DLA systems are determined by three processes operating in the gas of the host galaxy: (1) chemical evolution, due to the enrichment of the gas by stellar ejecta; (2) elemental depletion, caused by the incorporation of part of the metals into dust grains; and (3) ionization effects, produced by radiation fields penetrating the neutral gas. To the best of our knowledge, these are the only processes that can affect the measured abundances. In DLA systems, ionization corrections are generally smaller than the column density errors (e.g. Vladilo et al. 2001), with some exceptions (e.g. Prochaska et al. 2002) that we exclude from our samples. In our analysis, we therefore assume that the abundance ratios are uniquely determined by chemical evolution and elemental depletion, other effects being negligible.

2.2. Definitions from Galactic ISM studies

2.2.1. Depletions in the Galactic ISM

The elemental depletion of an element X is usually defined in logarithmic notation, with the expression

$$\delta_X = \log\left(\frac{X}{\rm H}\right)_{\rm gas} - \log\left(\frac{X}{\rm H}\right)_{\rm ref}, \quad (1)$$

where $(X/{\rm H})_{\rm gas}$ is the number ratio of atoms in the gas, and $(X/{\rm H})_{\rm ref}$ a reference value for the total number ratio (gas plus dust). In practice, the ratio in the gas is measured from the column densities of the dominant ionization stages in H I regions[4], i.e. $(X/{\rm H})_{\rm gas} = N(X_{\rm dom})/N({\rm H\,I})$. In Galactic ISM studies, the total ratio (gas plus dust) is assumed to be solar. This gives the empirical expression

$$\delta_X = \log\frac{N(X_{\rm dom})}{N({\rm H\,I})} - \log\left(\frac{X}{\rm H}\right)_{\odot}. \quad (2)$$

[2] Atomic nuclei do contribute to the X-ray cross section, but interstellar abundances based on X-ray spectroscopy are still very sparse even in the Galactic ISM (e.g. Ueda et al. 2005).

[3] In this work, we call *metallicity* the absolute abundance of a reference element X (e.g. zinc or iron), calculated as $[X/{\rm H}] \equiv \log(X/{\rm H}) - \log(X/{\rm H})_{\odot}$; we adopt the solar abundances of Asplund et al. (2005).

[4] For a list of dominant ionization stages in H I regions, we refer to Table 1 of Savage & Sembach (1996).

The depletions measured in this way are negative for most elements. This indicates that a fraction of the atoms is missing from the gas (Savage & Sembach 1996; Jenkins 2009). The strength of the depletion correlates with the *condensation temperature*, a quantity obtained from thermodynamical computations of particle condensation in a cooling gas of solar composition (Field 1974; Lodders 2003). The trend with condensation temperature suggests that the fraction of atoms missing from the gas is locked into dust grains.

2.2.2. Volatile and refractory elements

Refractory and volatile elements can be distinguished on the basis of either the depletion strength (Savage & Sembach 1996; Jenkins 2009) or the condensation temperature (Lodders 2003). For the purpose of our discussion, we recall that magnesium, silicon, and iron are classified as refractories; they have similar condensation temperatures ($T_{\rm cond} \approx 13 \times 10^2$ K) and all of them are depleted; however, the depletions of silicon and magnesium are milder than the depletion of iron (see Table 3). Zinc and sulfur are classified as volatile elements because they display negligible or small depletion and because they have low condensation temperatures ($T_{\rm cond} \approx 7 \times 10^2$ K).

2.3. Equations of the method

Equation (2) cannot be used to measure depletions in extragalactic studies because the assumption that the reference abundances are solar is not in general acceptable. A starting point in tackling this problem is to substitute hydrogen with a volatile element V, in Eq. (1). If the depletion of V is negligible, then $(V/{\rm H})_{\rm gas} = (V/{\rm H})_{\rm gas+dust} = (V/{\rm H})_{\rm ref}$ and Eq. (1) is equivalent to

$$\delta_X = \log\left(\frac{X}{V}\right)_{\rm gas} - \log\left(\frac{X}{V}\right)_{\rm ref} . \quad (3)$$

In this way, the measurement of the depletions relies on a set of *relative* abundances X/V (metal-to-metal), rather than *absolute* abundances $X/{\rm H}$ (metal-to-hydrogen). Relative abundances are less sensitive to chemical evolution than absolute ones and, in some cases, one can assume that relative abundances are solar even when the absolute abundances are not[5]. In general, however, this will not be true. In our method, we calculate sets of reference abundances $(X/V)_{\rm ref}$ for DLA galaxies, without relying on the solar abundance pattern.

The ratio (X/V) will vary in the course of chemical evolution. Since DLA host galaxies are observed at different stages of their history, we need to estimate a specific value of $(X/V)_{\rm ref}$ for each DLA system. We assume that the evolutionary state of the ith DLA galaxy can be deduced from the absolute abundance of the gas sampled by the line of sight. The volatile element is used to measure an absolute abundance unaffected by dust depletion $(V/{\rm H})_{O,i} \equiv N(V_{\rm dom})/N({\rm H\,I})$. To estimate $(X/V)_{\rm ref}$, we use a model of galactic chemical evolution developed for DLA galaxies, $\mathcal{M}$, that calculates (X/V) as a function of $(V/{\rm H})$. The value predicted by this model at $(V/{\rm H})_{\mathcal{M}} = (V/{\rm H})_{O,i}$ is adopted as the reference value of Eq. (3), i.e. $(X/V)_{{\rm ref},i} = (X/V)_{\mathcal{M},i}$. The depletions are calculated with the expression

$$\delta_{(X;V),i} = \log\left(\frac{X}{V}\right)_{O,i} - \log\left(\frac{X}{V}\right)_{\mathcal{M},i} , \quad (4)$$

where $(X/V)_{O,i} \equiv N(X_{\rm dom})/N(V_{\rm dom})$ is the ratio in the gas measured from the observed column densities.

2.4. Model constraints

A key point of the method is the choice of the models of galactic chemical evolution. To this end, we consider two volatile elements, V and V', that have a large number of column density measurements in DLA systems. We then use the observational diagram $(V'/V)_{O,i}$ versus $(V/{\rm H})_{O,i}$ as a dust-free diagnostic of the chemical evolution of DLA host galaxies. In practice, starting from a grid of models of galactic evolution, we select the model that minimizes the differences between the observed ratios, $(V'/V)_{O,i}$ and the ratios $(V'/V)_{\mathcal{M},i}$ predicted at $(V'/{\rm H})_{\mathcal{M}} = (V/{\rm H})_{O,i}$. Once a reference model is selected, we use its predictions $(X/V)_{\mathcal{M},i}$ to measure the depletions of refractory elements X with Eq. (4).

In principle, we can choose any pair of volatile elements when applying the method. In practice, zinc and sulfur are the only suitable choice to ensure a sufficient statistics (see Sect. 3). We therefore use the observed evolution of S/Zn versus Zn/H ratios to constrain the models. In the absence of other dust-free diagnostic tools of this kind, we also introduce an *age test* to restrict the choice of the models. This test exploits information on the age of DLA galaxies that can be obtained by their absorption redshifts. The detailed implementation of the method is presented in Sect. 5.1.

2.5. Caveats from Galactic ISM studies

2.5.1. Zinc and sulfur depletion

No element is perfectly volatile and zinc and sulfur are no exception. In highly depleted Galactic lines of sight, these elements also appear to be depleted (Savage & Sembach 1996; Jenkins 2009). Since DLA systems are generally dust-poor, zinc and sulfur will be undepleted in most cases. However, they can be depleted in some DLA systems and we must assess the consequences of this effect on our method. To identify dust-rich systems, we use the molecular fraction $f({\rm H_2}) \equiv 2\,N({\rm H_2})/[N({\rm H\,I} + 2\,N({\rm H_2})]$. This quantity correlates with depletion in both the ISM (e.g. Savage & Sembach 1996) and DLA systems (e.g. Noterdaeme et al. 2008). Even zinc and sulfur could be depleted in lines of sight with high $f({\rm H_2})$. Chemical pathways that may lead to sulfur depletion in molecular clouds were discussed by Scappini et al. (2003).

If present, zinc and sulfur depletion would affect our procedure at two stages: first in the selection of the models of galactic chemical evolution and then in the measurements of the depletions.

In the first stage, the presence of zinc and sulfur depletion would affect the process of minimization of the χ^2 defined in Eq. (6). Since the critical quantity in this process is the *ratio* S/Zn, the procedure would be mainly affected by the *differential* depletion between zinc and sulfur. To the extent at which the depletions of these two elements track each other, the differential depletion may be negligible. In any case, to minimize the impact of zinc or sulfur differential depletion on our procedure, we excluded molecular DLA systems during the stage of model selection. More details are given in Sect. 5.1.

After the models are selected, the presence of zinc and/or sulfur depletion would affect the measurements of the depletions

[5] As an example, depletions in the SMC were estimated by assuming $(X/{\rm Zn})_{\rm ref} \simeq (X/{\rm Zn})_\odot$ or $(X/{\rm S})_{\rm ref} \simeq (X/{\rm S})_\odot$ (Welty et al. 2001; Sofia et al. 2006). The relative abundances of SMC stars are roughly solar, despite the low metallicity of the SMC ([Fe/H] $\simeq -0.6/-0.7$ dex).

of the refractory elements. If the depletion of the volatile element, $\delta_{V,i}$, is not negligible, Eq. (4) should be re-written as

$$\delta_{X,i} = \log\left(\frac{X}{V}\right)_{O,i} - \log\left(\frac{X}{V}\right)_{\mathcal{M},i} + \delta_{V,i}. \quad (5)$$

To derive $\delta_{X,i}$, one could model the unknown value of $\delta_{V,i}$ by using a scaling law between $\delta_{V,i}$ and $\delta_{X,i}$ based on Galactic ISM studies, and solving the equation by iterations (e.g. Vladilo 2004). However, in the present work we prefer not to use relations between the depletions obtained from Galactic ISM studies. These relations might not hold in the very first stages of dust production, when the chemical processes determining the dust composition might differ from the present-day ones. In any case, we expect $\delta_{\rm Zn}$ and $\delta_{\rm S}$ to be small in most cases, with the exception of molecular DLA systems. In these cases, zinc and sulfur could be depleted and the depletions of refractories calculated with Eq. (4) should be considered a lower limit to the true value.

2.5.2. Sulfur abundances in partially ionized regions

In some Galactic lines of sight, the interstellar S/H ratio has peculiar values, apparently in excess of the solar ratio (Jenkins 2009). Before using sulfur as a reference element for our analysis, we investigated the reason for this behavior. An explanation can be found in terms of ionization effects. Owing to the large difference between the ionization potentials of S II (23.3 eV) and H I (13.6 eV), S II can be the dominant state of sulfur in partially ionized regions, where a fraction of H I is converted to H II. Therefore in partially ionized regions the total H, calculated from H I, is underestimated and the ratio S/H overestimated. According to this explanation, the apparent S/H excess should only appear along lines of sight with low N(H I) column density, typical of partially ionized regions. Indeed, by using Jenkin's database (Tables 2 and 13 of that paper), one can see that the anomalous ratios (e.g. $[{\rm S_{gas}/H}] \gtrsim +0.2$ dex) are only found when $N({\rm H\,I}) \lesssim 10^{19.5}$ cm^{-2}. We conclude that this effect is not a reason of concern in our analysis because we consider absorption systems with high H I column density, $N({\rm H\,I}) \geq 10^{20.1}$ cm^{-2}, which are typical of neutral regions.

3. The data

The present study requires a large database of DLA column densities: for the volatile elements, we need a good coverage in metallicity to constrain the models of chemical evolution; for the refractory elements, we need many measurements to characterize the depletion properties as a function of metallicity and redshift. It is only thanks to the accumulation of high quality literature data that this task has become possible.

The number of column-density measurements that has been accumulated for the refractory elements is generally much higher than that of the volatiles. Among the refractories, we consider here silicon, the focus of the present investigation, and iron, for the sake of comparison with previous studies of depletion in DLA systems. In addition, we consider magnesium, another important ingredient of silicates poorly investigated in DLA systems. Silicon and magnesium are expected to behave similarly because they have similar condensation temperatures (Lodders 2003) and Galactic depletions (Savage & Sembach 1996). Therefore, magnesium results, even if scarce, can be used as an independent cross check of silicon results.

The dominant ionization states of magnesium, silicon, and iron are Mg II, Si II and Fe II. The number of Si II and Fe II measurements is large because these ions have enough transitions to cover a wide range of wavelengths and oscillator strengths. The wavelength coverage translates into a good coverage of absorption redshift; the range of oscillator strengths yields accurate measurements, unaffected by saturation, over a wide interval of metal column density. The number of Si II and Fe II DLA column densities currently available is 131 and 167, respectively, with the selection criteria specified in Sect. 3.2. The number of reliable measurements of Mg II is very small because the resonance doublet at ≃280 nm is usually saturated. We therefore used measurements obtained from the doublet at 124 nm, which is hard to detect because it is weak and falls inside the Ly α forest of the quasar spectrum. We only found data for ten DLA systems. This small number is still sufficient for comparison purposes.

The bottleneck in our procedure is the number of available column densities of the volatile elements, which are essential for constraining the models and measuring the depletions. The two dominant ions of volatile elements with the largest number of accumulated measurements are Zn II and S II, with a total of 94 and 64 data, respectively (excluding our S II data presented below). The only Zn II usable transitions fall at $\lambda\lambda$202.6, 206.2 nm in the rest frame. These lines are generally unsaturated, but can be too faint in DLA systems of low metal column density. The S II lines fall at $\lambda\lambda$125.0, 125.3, 125.9 nm. The presence of these three lines in the same portion of the spectrum, with a good coverage of oscillator strengths, makes it possible to obtain accurate S II column densities despite these lines falling inside the Ly α forest.

The combined zinc-sulfur sample (33 DLA systems without our S II measurements) does not have a perfect match in redshift because the Zn II lines are easier to detect at $z_{\rm abs} \lesssim 3$, while the S II lines can only be detected at $z_{\rm abs} \gtrsim 2$ with ground-based instrumentation. This non-ideal coverage in redshift is not a severe limitation for the application of our method, since the models are constrained in metallicity rather than in redshift. The metallicity interval spanned by the combined Zn II + S II sample covers most of the metallicities observed so far in DLA systems, which are concentrated in the interval $-2 \lesssim [{\rm Zn/H}] \lesssim 0$, with a few exceptions.

Since S II is currently the bottleneck, we performed an extensive analysis of archive spectra to obtain new measurements of N(S II). We report below the results of this search. In Sect. 3.2, we present the literature database.

3.1. New measurements of S II column densities

In our search for new measurements of S II column densities, we used the ESO archive of spectra collected with the UVES spectrograph fed by the unit 2 of the ESO VLT (Very Large Telescope) at Cerro Paranal (Chile). The high spectral resolution ($R = \lambda/\Delta\lambda \simeq 5 \times 10^4$) combined with high spectral coverage and high efficiency in the visible ultraviolet makes this instrumentation particularly well suited to searching for lines in the Lyman α forest, as in the case of S II lines at $\lambda \simeq 125$ nm.

From our search of the ESO archive, we found UVES spectra relative to 18 DLA systems with unpublished S II data. We analyzed these spectra with the MIDAS software package developed at ESO. An average spectrum was derived from the multiple spectra present in the archive for each DLA system. The average spectra were normalized to the local continuum of the quasar. For more details on the analysis of these UVES spectra we refer to previous work of ours (e.g. Centurión et al. 2003). The column densities were derived by fitting the normalized spectrum with the Voigt-profile fitting routines FITLYMAN (Fontana & Ballester 1995) implemented in MIDAS. Oscillator

Table 1. New S II column density measurements obtained from the Voigt fitting analysis of archive UVES spectra.

QSO	z_{qso}	z_{abs}	log N(H I)	r(H I)[a]	n_{sp}[b]	Ion	log N(X)	Transitions used in the fit
0216+080	2.992	2.2930	20.50 ± 0.10	26e	8	Fe II	14.88 ± 0.02	1608.4511 & 2374.4612 Å
						S II	15.04 ± 0.02	1253.805 & 1250.578 Å
2206-199A	2.559	1.9200	20.68 ± 0.03	21i	7	Fe II	15.31 ± 0.01	2249.8768 & 2260.7805 Å
						S II	15.42 ± 0.02	1250.578 & 1259.518 Å
2359-0216	2.810	2.0950	20.65 ± 0.10	26e	4	Fe II	14.55 ± 0.07	2374.4612 Å
						S II	[15.28 ± 0.07][c]	1250.578 Å

Notes. [(a)] Reference code for H I column density. Codes are specified in Table 7; [(b)] number of UVES archive spectra averaged; [(c)] noisy spectrum contaminated by forest. Uncertain value not used in subsequent analysis.

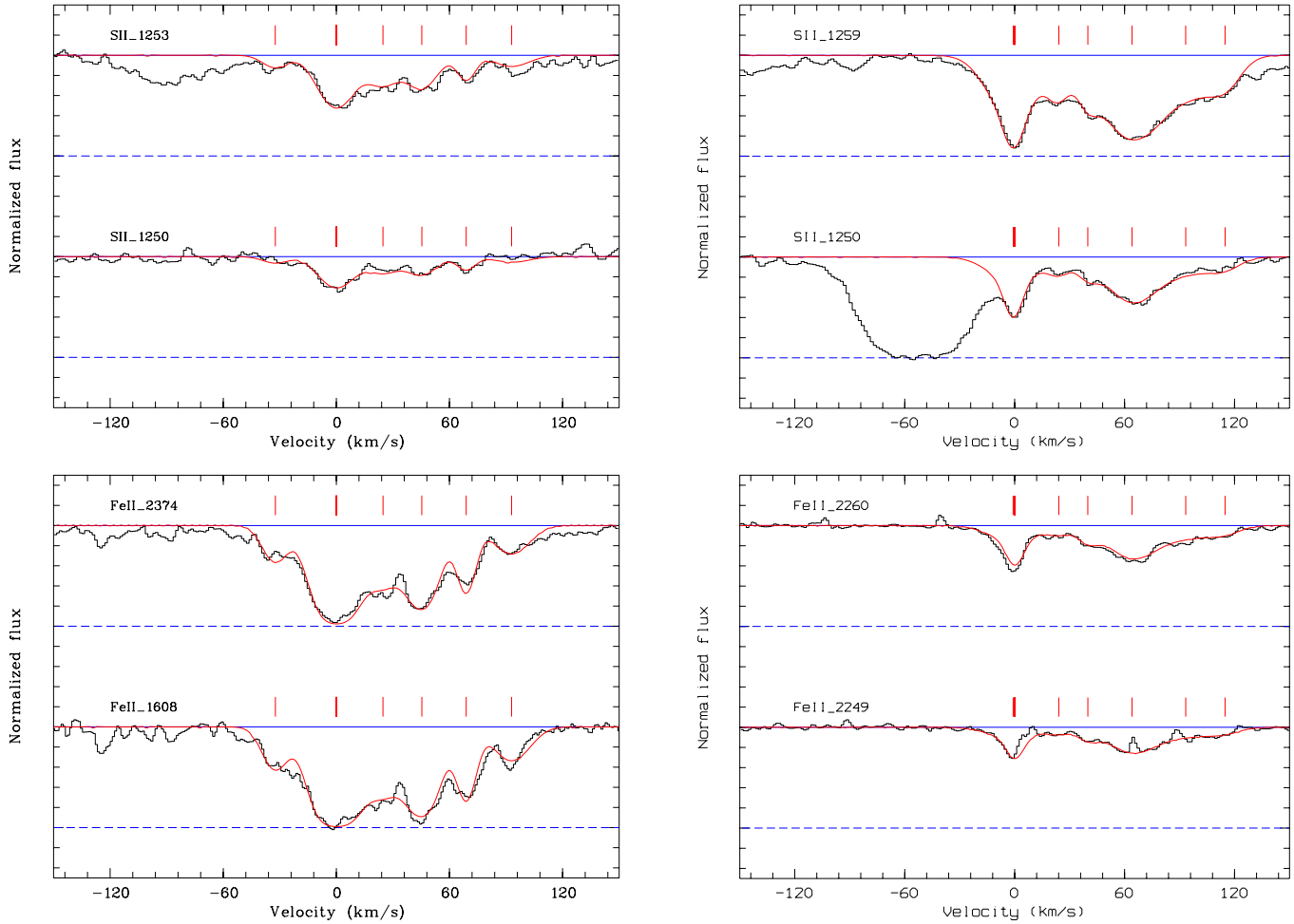

Fig. 1. Multi-component Voigt profile fits of S II and Fe II lines for the DLA systems at z_{abs} = 2.2930 in Q0216+080 (*left panels*) and at z_{abs} = 1.9200 in Q2206-199 (*right panels*). In each spectral region, we indicate the ion and rest-frame wavelength of the transition; the continuum and zero levels are indicated with solid and dashed lines, respectively. The radial velocity scale is obtained from the wavelength scale using the redshift of the strongest absorption component of each system as a reference. The velocity components used in the fits are marked with vertical ticks. The positions of the S II velocity components (*top panels*) were constrained from the analysis of Fe II lines outside the Ly α forest (*bottom panels*). The spectral region around the redshifted 2249 Å Fe II lines in Q2206-199 (*bottom right panel*) is disturbed by a few cosmic events (emission spikes).

strengths for the transitions of interest were taken from Morton (2003).

We detected S II in 3 of the 18 systems analysed. The results of these systems are shown in Table 1. For two of them, we found a clear detection in at least two lines of the S II triplet, as we show in Fig. 1. The column densities were obtained by fitting the multiple absorption components seen in each DLA system. The quoted column-density errors, provided by FITLYMAN, do not include uncertainties associated with the tracing of the continuum. The redshift position of each S II component was constrained from the analysis of Fe II lines outside the Ly α forest. The comparison between S II and Fe II normalized profiles was also used to check for potential contamination of Lyα forest. The Fe II column density was also measured as a cross-check

with previous work. The Fe II measurements that we find are in good agreement with previous measurements in the same systems.

For a third DLA system, $z_{abs} = 2.0950$ in Q2359-0216, we did detect the S II line at 125.0 nm, but not the other two lines in the same range, owing to contamination by the forest. In this case, the quality of the spectra was also lower. The S II measurement of this system was not considered in the subsequent analysis.

3.2. The column density database

The data used in this work were selected from 293 DLA systems with published measurements of column densities. These include the data presented in Table 1. Only measurements were considered, rather than lower or upper limits. Most of the original observations were obtained at high spectral resolution, $R \approx \lambda/\delta\lambda \simeq 5 \times 10^4$, with the UVES spectrograph, at the unit 2 of the ESO Very Large Telescope, and with the HIRES spectrograph at the Keck telescope. Data obtained from low-resolution spectra (e.g. SDSS spectra) were not considered. More details on the observational data can be found in the original papers listed in Table 7. Here we explain the criteria followed to build the database.

We considered all quasar absorption systems with $N(\mathrm{H\,I}) \geq 10^{20.1}$ cm^{-2}. This threshold is slightly lower than the classical limit that defines DLA systems, i.e. $N(\mathrm{H\,I}) \geq 10^{20.3}$ cm^{-2} (Wolfe et al. 1995). By relaxing this limit, we have been able to include in our sample eight "sub-DLA" systems that allow us to probe the high end of the metallicity distribution (Péroux et al. 2007; Prochaska et al. 2006). Most sub-DLAs in our sample have $N(\mathrm{H\,I})$ consistent with the classic DLA limit within the errors. For simplicity, we refer to as DLA systems all the quasar absorbers of our sample.

A reason of concern in our analysis is the possible presence of ionization effects that could alter the measured abundances. Therefore, while collecting the column density data, we searched the literature for reports of ionization studies. As a result, we discarded from our sample two cases affected by ionization, namely the systems at $z_{abs} = 2.625$ in GB 1759+7539 (Prochaska et al. 2002) and at $z_{abs} = 2.067$ in Q0450-13 (Dessauges-Zavadsky et al. 2006). We checked with particular attention the systems with lowest values of $N(\mathrm{H\,I})$, for which ionization could be more relevant. However, we did not find any evidence of enhanced ionization effects in our sample of sub-DLA systems. In constrast, for the system at $z_{abs} = 1.768$ in Q0953+5230, the measured Al^{++}/Si^{+} ratio is consistent with predominantly neutral gas (Prochaska et al. 2006). This system is particularly important for constraining the high end of the metallicity evolution in our models of galactic chemical evolution.

While assembling the database, we also checked for proximate DLA systems (PDLAs) with $z_{abs} \simeq z_{qso}$, which in principle could be severely ionized by the radiation of the nearby quasar. Detailed studies of individual PDLAs have not revealed peculiar ionization effects (Møller et al. 1998; Rix et al. 2007). The most recent study of abundances in PDLAs reports some evidence of enhanced ionization, particularly at low $N(\mathrm{H\,I})$; however, no distinct trends are found in Zn/Fe and Si/Fe abundance ratios compared with intervening DLAs (Ellison et al. 2010). In our accumulation of literature data, we found several PDLAs with relative velocity separation from the quasar $\Delta V < 3000$ km s^{-1}. For our analysis, we kept five cases with $\Delta V > 1000$ km s^{-1} and $\log N(\mathrm{H\,I}) \gtrsim 20.7$ and rejected the other cases more prone to ionization effects. The five PDLAs in our sample yield results generally in line with intervening DLA systems (see e.g. Fig. 5).

The metal column densities that appear in the literature are measured with two methods: Voigt profile fitting and the *apparent optical depth* (AOD) method (Savage & Sembach 1991). In the absence of saturation, these two methods yield identical values of total metal column density. With the Voigt method, it is possible to solve the multiple-component velocity structure generally present in the absorption profiles of the metals. However, this structure cannot be solved in the H I profiles and for this reason we are interested in the *total* column density of the metals, the only one that can be compared to $N(\mathrm{H\,I})$ in the abundance ratios. When a detailed multiple component analysis was reported by the authors, we checked that the bulk of the column density of interest originated in the same velocity components.

The errors in the metal column densities quoted in the literature, σ_m, generally take into account the statistical noise of the measurements, but no other uncertainties, such as the error in the continuum tracement. For this reason, values of $\sigma_m \simeq 0.01$ dex, or even smaller, are sometimes reported. These errors are sometimes unrealistic, in which case they tend to overestimate the true χ^2 (Eq. (6)). To reduce this effect, we used the published error when $\sigma_m \geq 0.02$ dex and adopted instead a minimum value of 0.02 dex in the other cases. This criterion was also consistently applied to our new measurements shown in Table 1.

3.3. Observational samples

We refer to as the "(Zn+S) sample" the set of DLA systems with both S and Zn column density measurements. These are the systems for which we can fully apply our method. In addition to this sample, we also considered DLA systems with either Zn or S column densities available, but not both of them. For these systems, it is still possible to apply our method with some limitations described below.

For brevity, we refer to as the "$\mathcal{Z}$ sample" the set of DLA systems with Zn II (but not S II) data and the "$\mathcal{S}$ sample" the set of DLA systems with S II (but not Zn II) data. The advantage of using the $\mathcal{Z}$ and $\mathcal{S}$ samples is twofold: we can increase the statistics and probe a larger redshift interval (Fig. 6). The (Zn+S), $\mathcal{Z}$ and $\mathcal{S}$ samples are listed in Tables 4–6, respectively. These samples contain 35, 47, and 29 DLA systems, respectively, including our S II data. For each absorber, we give the column densities of the volatile elements and references for the literature sources consulted for both volatile and refractory elements.

4. Models of galactic chemical evolution

Our choice of chemical evolution models was based on previous studies of the nature of DLA systems. This has been the subject of intense debate in the literature owing to the difficulty of revealing the nature of the absorbing galaxies on pure observational grounds.

Direct imaging of the field of the background quasar should ideally reveal the morphology of the intervening galaxies. Unfortunately, it is extremely difficult to solve the galaxies from the quasar light and to choose between different candidate galaxies present in the same field. At intermediate redshift ($z_{abs} \lesssim 1$), where this task is more feasible, the DLA candidate galaxies show a variety of morphological types, spirals not being predominant (Le Brun et al. 1997). At higher redshifts ($z_{abs} \gtrsim 2$), where most known DLA systems are found, the observations are rather

sparse and generally consistent with these systems being objects of low emissivity and low rates of star formation (Weatherley et al. 2005; Péroux et al. 2011).

Studies of high-resolution absorption-line spectra cast light on the kinematics and the chemical abundances of DLA galaxies. However, kinematical studies are not conclusive: the statistics of the radial-velocity profiles is consistent with a variety of possible origins, ranging from progenitors of present-day spirals (Prochaska & Wolfe 1997) to proto-galactic clumps (Haehnelt et al. 1998).

Studies of chemical abundances have tried to solve this issue by comparing DLA abundance ratios with ratios observed in stars or galaxies of similar metallicity. In particular, the ratio of α-capture to iron-peak elements has been used to constrain the chemical history of DLA galaxies. The high values of the Si/Fe ratio at low metallicity observed in DLA systems, if taken at face value, are consistent with these systems being possible progenitors of the Milky Way (e.g. Lu et al. 1996). However, differential depletion is likely to enhance the Si/Fe ratios and the study of dust-free α/Fe ratios suggests that DLA systems behave differently from metal-poor Milky Way stars (e.g. Centurión et al. 2000; Vladilo 2002).

Models of galactic chemical evolution have been used to cast light on the history of the chemical enrichment of DLA galaxies (e.g. Matteucci et al. 1997; Jimenez et al. 1999; Prantzos & Boissier 2000b). To cope with the problem of differential depletion, dust-corrected abundances have been used in some studies (e.g. Calura et al. 2003). These studies together imply that DLA systems originate in galactic regions with low rates of star formation, such as dwarf galaxies or external regions of spirals (e.g. Dessauges-Zavadsky et al. 2004). An origin in elliptical galaxies is ruled out.

The motivation behind the present work is not to determine conclusively the nature of DLA galaxies but to calculate the implications in terms of depletions of different, plausible models of chemical evolution of DLA galaxies. In our choice of the models, we considered both dwarf irregular galaxies, with a broad range of parameters, and spiral galaxies, without making any selection a priori. We then used our methodology to select the models that most closely reproduce the observational trend S/Zn versus Zn/H. The models differ in their star formation histories, but share the same, up-to-date nucleosynthetic prescriptions: stellar yields were taken from François et al. (2004). We chose these yields because they were tuned to reproduce at best the abundance patterns in the Milky Way. In the case of sulfur, we calculated the yield by using the same procedure followed by François et al. (2004). We now introduce the main features and parameters of the models. The process of model selection is explained in Sect. 5.1.

4.1. Models of spiral galaxies

The models for spiral galaxies are based on the chemical evolution model of the Milky Way (Chiappini et al. 1997). The Galaxy is assumed to have formed by means of two main infall episodes: the first forms the halo and the thick disk, the second the thin disk. The formation of the thin disk is assumed to be a function of the galactocentric distance, leading to an inside-out scenario for the Galaxy disk build-up (Matteucci & François 1989). The Galactic disk is approximated by several independent rings, 2 kpc wide, without any exchange of matter between them, and for each ring we compute the chemical evolution.

This model has been revised with time to reproduce an extended set of observational constraints, in particular the G-dwarf metallicity distribution and various relations between the abundances of metals (C, N, O, α-capture elements, iron-peak elements) as functions of the [Fe/H] abundance (see François et al. 2004; Chiappini et al. 2006; and Cescutti et al. 2009). Although this model is not the only one capable of reproducing the data, it does reproduce the majority of the Milky Way properties, and most of its assumptions are shared by other authors (e.g. Prantzos & Boissier 2000a; Alibés et al. 2001; Chang et al. 1999). By adopting this model for other spiral galaxies, most of the parameters are fixed by the observational constraints of the Milky Way. The advantage is that many features of the model are well constrained.

In our application of the Milky Way model to DLA host galaxies, we took into special consideration the assumptions that may influence the abundance ratios in the external parts of the disk. In fact, if some DLA galaxies are spirals, geometrical considerations indicate that the random line of sight to the quasar will intersect the external regions more probably than the internal ones. As Chiappini et al. (2001) have shown, the chemical evolution of the halo can have an impact on the abundance gradients in the outer parts of the disk. In their model A, the halo surface mass density is assumed to be constant (=17 $M_{\odot}$ pc^{-2}) for galactocentric distances $R_{\rm GC} \leq 8$ kpc and to decrease outwards as $R_{\rm GC}^{-1}$. Their model B has instead a constant value (=17 $M_{\odot}$ pc^{-2}) for all the galactocentric distances. The differences among model A and B arise primarily in the predicted evolution for the outermost regions of the disk. In these regions, the model B predicts the flattest gradients and provides the best fit to recent observations of Cepheids stars (see Cescutti et al. 2007) and distant open clusters, whereas model A is in good agreement with the steeper gradients traced by planetary nebulae (see Chiappini et al. 2001). In the present work, we decided to compare the DLA data with the results of both models for the evolution of external rings. We also considered two different types of stellar initial mass function (IMF): the Scalo IMF (Scalo 1986), which gives the best results for the Milky Way observational constraints, and the Salpeter IMF (Salpeter 1955), for the sake of comparison with the models of dwarf galaxies discussed below.

In summary, for each of the two Milky Way models A and B we calculated the abundance ratios of interest in eight rings of galactocentric distance between 4 and 18 kpc. These computations were performed with the Scalo IMF and repeated with the Salpeter IMF. In this way, we obtained 32 sets of model predictions of spiral galaxies. More details on the adopted Milky Way model can be found in Chiappini et al. (2001).

4.2. Models of dwarf irregular galaxies

The chemical evolution model of dwarf galaxies is an updated version of the one-zone model developed by Bradamante et al. (1998) to study the formation and evolution of late-type dwarf galaxies, dIrrs, and BCDs. The model assumes that the galaxy is built up by continuous infall of primordial gas.

Stars form and later contaminate the ISM with their products of nucleosynthesis, which mix instantaneously and completely with the ISM. Stellar lifetimes are taken into account in detail, i.e. the instantaneous recycling approximation (IRA) is relaxed. Part of the energy released by supernovae (SNe) and stellar winds is deposited into the ISM, and galactic winds develop when the thermal energy of the gas exceeds its binding

Table 2. Parameters of the models of dwarf galaxies.

Parameter	Range of values
$M_{\rm infall}$ ($M_\odot$)	1×10^9, 5×10^9
ϵ (Gyr^{-1})	0.05; then from 0.1 to 1.0 at steps of 0.1
Wind type[a]	normal[b] , metal enhanced[c]
λ_w (Gyr^{-1})	from 0 to 10 at steps of 0.5

Notes. [(a)] The case of no wind corresponds to $\lambda_w = 0$; [(b)] same wind efficiency for all elements: $w_{\rm H,He} = w_i = 1$; [(c)] higher wind efficiency for metals: $w_{\rm H,He} = 0.3$, $w_i = 1$.

energy. The wind expels metals from the galaxy, hence it has a significant influence on the history of chemical enrichment of the galaxy.

In the present application of the model, the rate of gas infall is assumed to exponentially decrease with time, with a time scale $\tau = 1$ Gyr. A Salpeter IMF with index $x = 1.35$ is adopted. The chemical evolution is calculated as a function of time and the computations are stopped after 13 Gyr. The total quantity of infalling gas accreted throughout the lifetime of the galaxy is fixed by the parameter $M_{\rm infall}$. Changes in $M_{\rm infall}$ are expected to affect the absolute value of gas and stellar mass, but have a negligible effect on the abundance ratios. In this respect, models with different values of $M_{\rm infall}$ are self-similar before the wind blows. Even if abundance ratios depend weakly on $M_{\rm infall}$, we considered two possible values of $M_{\rm infall} = 1 \times 10^9\ M_\odot$ and $5 \times 10^9\ M_\odot$. If we only adopt the smaller value, the galaxy mass will become too low in the case of a strong galactic wind. To cover the whole mass range of dwarf galaxies, we chose to also experiment with the higher value.

The evolution of the abundance ratios is mostly affected by the efficiency of star formation and the possible presence of galactic winds. We therefore considered a broad range of values for the parameters that describe these effects. The star formation efficiency (SFE) is specified by the parameter ϵ, while the strength of the wind is given by $w_i\lambda_w$, where w_i is a weight parameter that is specific to each chemical element. By changing w_i, we can consider normal winds, with $w_{\rm H,He} = w_i = 1$, and metal-enhanced winds, where the wind efficiency of metals is enhanced for some specific elements (for example metals), i.e. $w_i > w_{\rm H,He}$. Both parameters ϵ and λ_w are expressed here in units of Gyr^{-1} (Yin et al. 2010).

The combinations of model parameters that we adopted are summarized in Table 2. A total of 11 star formation efficiencies and 21 wind strengths were considered, in conjunction with two possibles values of $M_{\rm infall}$ and two types of wind. From these, we computed a grid of 924 models. The broad range of star formation efficiencies and wind strengths allow us to explain the possibility that DLA systems originate in a variety of dwarf galaxies, including dwarf irregulars, low surface brightness, and dwarf spheroidals. A complete description of the model equations and parameters can be found in Yin et al. (2010).

5. Application of the method

We present the main steps followed in the application of our method: (1) the selection of chemical evolution models based on the abundances of volatile elements; (2) the comparison of measured and predicted abundance ratios of refractories and; finally, (3) the calculations of depletions. The resulting depletions are discussed in Sect. 6.

5.1. Selection of the chemical evolution models

5.1.1. Data used for the model selection

The DLA systems used to constrain the models are shown with filled diamonds in Fig. 2 and listed in the first part of Table 4. The other systems displayed in the same table were temporarily excluded from the process of model selection but used in the rest of the analysis. One case (last row in Table 4, square symbol in Fig. 2) was excluded because it shows a peculiar nucleosynthetic behavior, with Ti, Ni, and Zn abundances anomalous relative to any other DLA or metal-poor Galactic star (Cooke et al. 2010). Molecular DLA systems (second part of Table 4, filled circles in Fig. 2) were excluded because they may be affected by zinc/sulfur differential depletion, as we explained in Sect. 2.5.1. To this end, we used the results of the VLT/UVES DLA molecular survey (Noterdaeme et al. 2008, and refs. therein). Systems with $f(H_2) > 10^{-4.5}$ were not used to constrain the models. This threshold was proposed by Noterdaeme et al. (2008) to separate systems with high molecular content. The majority of the data sample that we use has been surveyed for H_2 and is proven to have low molecular content, i.e. $f(H_2) < 10^{-4.5}$. However, for 11 systems of this sample there is no measurement of $f(H_2)$. Given the low rate of incidence of molecular systems with $f(H_2) > 10^{-4.5}$ ($\simeq$14% in the VLT/UVES survey), we expect only one or two out of these 11 systems to be molecular. In order to have a larger statistics, we kept these DLA systems in the sample.

5.1.2. Criteria adopted for the model selection

To select the models, we calculated the reduced χ^2 obtained by comparing observations and models in the diagram S/Zn versus Zn/H given by

$$\chi^2_\nu = \frac{1}{\nu} \sum_{i=1}^{n} \frac{[\log({\rm S/Zn})_{O,i} - \log({\rm S/Zn})_{\mathcal{M},i}]^2}{\sigma^2_{O,i}}, \quad (6)$$

where $({\rm S/Zn})_{O,i} = N_i({\rm S\,II})/N_i({\rm Zn\,II})$ is the observed column-density ratio, $({\rm S/Zn})_{\mathcal{M},i}$ the ratio predicted by the model at $({\rm Zn/H})_{\mathcal{M}} = ({\rm Zn/H})_{O,i}$, and $\sigma_{O,i}$ is the measurement error in $\log({\rm S/Zn})_{O,i}$. The number of degrees of freedom is $\nu = n - n_{\rm par}$, where n is the number of DLA systems of the data set that satisfy the age test described below, and $n_{\rm par}$ is the number of parameters that are changed in the process of model selection.

The *age test* can be explained as follows. Each model $\mathcal{M}$ gives the abundances X/H as a function of the time elapsed since the beginning of star formation, $\Delta t_{\mathcal{M}}$. From this, we calculate the $\Delta t_{\mathcal{M},i}$ predicted by the model at the observed abundance Zn/H or S/H of the ith DLA system. We then calculate the look back time of the system, $t_i(z_{\rm abs})$, from its absorption redshift and a set of cosmological parameters. At this point, we estimate the look back time of the beginning of star formation implied by the model, $t_{\mathcal{M},i}(0) = t_i(z_{\rm abs}) + \Delta t_{\mathcal{M},i}$. Finally, we impose that $t_{\mathcal{M},i}(0) \leq t_{\rm reion}$, where $t_{\rm reion}$ is the look back time of the epoch of cosmic reionization. From this condition, we obtain the constraint

$$\Delta t_{\mathcal{M},i} \leq t_{\rm reion} - t_i(z_{\rm abs}). \quad (7)$$

In the calculations of look-back time and $t_{\rm reion}$, we adopt $H_0 = 71.9$ km s^{-1} Mpc^{-1}, $\Omega_{\rm m} = 0.258$, and $z_{\rm reion} = 11.0$ (Dunkley et al. 2009), and we allow for an uncertainty of 0.5 Gyr in the cosmic age scale. Any representative model of DLA galaxies should satisfy the condition given in Eq. (7), within the errors, for most of the DLA systems of the sample. In practice,

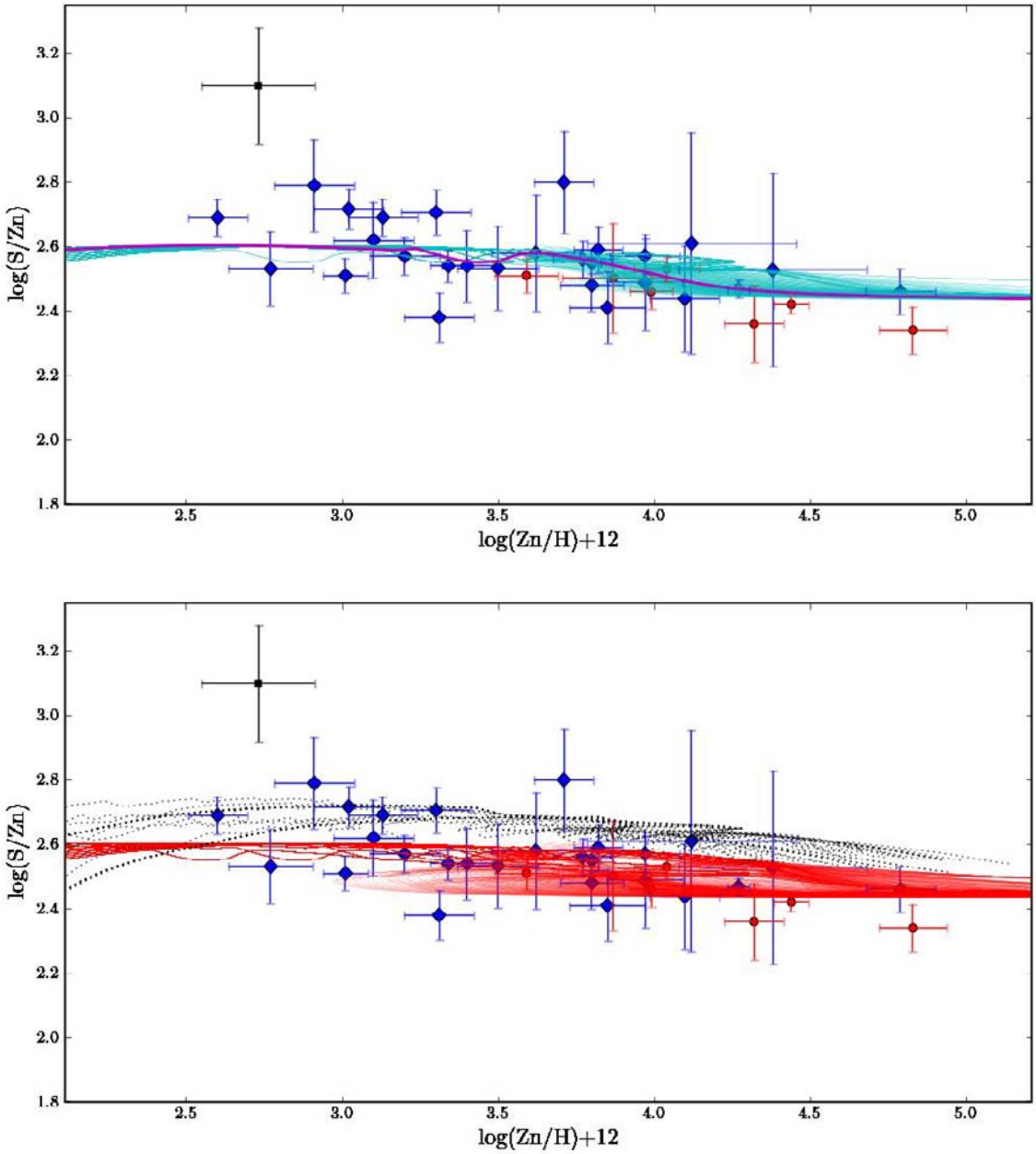

Fig. 2. Abundance ratios S/Zn versus Zn/H in DLA systems. *Symbols with error bars*: measurements for the samples of DLA systems listed in Table 4; *curves*: predictions of the models of galactic chemical evolution presented in Sect. 4. Blue diamonds: sample used to select the models of galactic chemical evolution (first part of Table 4); red circles: molecular DLA systems (second part of Table 4); black square: DLA system with peculiar nucleosynthetic abundances (last row in Table 4). *Top panel*: thin, cyan curves: models that pass the χ^2_ν selection condition (Eq. (8)); thick, magenta curve: best-fit *reference* model. *Bottom panel*: solid, red curves: dwarf models rejected by the χ^2_ν selection process; black, dotted curves: Milky Way models rejected by the χ^2_ν selection process.

we selected models for which ≥95% of the DLA systems satisfy the test.

5.1.3. Results of the model selection

With the above discussed criteria, we selected the models that satisfy the condition

$$\chi^2_\nu < \chi^2_{\nu,0.05}, \tag{8}$$

where $\chi^2_{\nu,0.05}$ is defined in such a way that the probability of χ^2_ν exceeding $\chi^2_{\nu,0.05}$ is $P(\chi^2_\nu > \chi^2_{\nu,0.05}) = 0.05$ (see e.g. Bevington & Robinson 1992). The models that do not satisfy this condition have a probability >95% of not being representative of the observational sample.

From this selection, we found 322 models of dwarf galaxies; their tracks are shown as thin, cyan curves in the top panel of Fig. 2. The tracks of the rejected models are shown in the bottom panel of the same figure; these include the remaining 602 dwarf models (red, solid curves) and all the 32 Milky-Way models (black, dotted curves).

The SFE of the selected dwarf models lie in the range $0.3 \leq \epsilon \leq 1.0$ Gyr^{-1}, with a median value $\epsilon = 0.4$ Gyr^{-1}. The wind strength covers the full range considered, i.e. $1.0 \leq \lambda_w \leq 5.5$ Gyr^{-1}, with a median value $\lambda_w = 3.5$ Gyr^{-1}. The wind type is generally normal rather than metal-enhanced. Most of these

models have $M_{\rm infall} = 1 \times 10^9\ M_\odot$, and only two of them have $M_{\rm infall} = 5 \times 10^9\ M_\odot$.

Among the selected models, the model with minimum χ^2_ν is shown as a thick magenta curve in Fig. 2; its reduced chi-square is $\chi^2_\nu = 1.34$. This best-fit model is that of a dwarf galaxy with parameters $M_{\rm infall} = 1 \times 10^9\ M_\odot$, $\epsilon = 0.4\ {\rm Gyr}^{-1}$, and normal wind with $\lambda_w = 3.5\ {\rm Gyr}^{-1}$.

We adopt the best-fit model as a *reference model* to calculate the reference abundances $(X/V)_{\mathcal{M},i}$ and derive the depletions with Eq. (4). We use the rest of the selected models to estimate the spread of the reference abundances $(X/V)_{\mathcal{M},i}$ at the value of metallicity of the ith DLA system. By taking into account the spread of the selected models in the error propagation (Eq. (9)), we acknowledge that DLA galaxies may undergo different chemical evolution histories. The selected models cover a broad range of physical parameters representative of quite different types of galaxies.

The reference model fits 60% (21/35) of all the DLA systems of Table 4 at $\leq 1\sigma$ level and 94% (33/35) at $\leq 2\sigma$ level. These figures indicate the extent to which this best-fit model is representative of DLA systems selected with our criteria. The reference model is certainly not the unique answer about the nature of DLA host galaxies, but it is a practical tool useful for the calculations of depletions. In this spirit, we present in Table 8 the evolutionary tracks predicted by the reference model for the abundances of Mg, Si, S, Fe, and Zn. The full version of the tracks is available in electronic form.

5.1.4. Comments on the model selection

The seven molecular DLA systems not used in the χ^2 minimization are plotted with red circles in Fig. 2. Most of their deviations from the reference model (6 out of 7) are negative, which hints at the presence of some systematic effect (possibly differential sulfur/zinc depletion, as we later discuss in Sect. 6.5). The possibility of a systematic effect supports our choice of excluding molecular systems during the χ^2 minimization. However, the magnitude of this effect is so small that molecular systems are almost indistinguishable from the rest of the sample. The reference model fits 43% of molecular systems (4/7) at the 1σ level and 100% (7/7) at the 2σ level. Since the differences between molecular and non-molecular systems are small, we expect differential sulfur/zinc depletion to be consequently small. This conclusion is true a fortiori for the non-molecular sample that we used to model the chemical evolution of the S/Zn ratio. We conclude that differential sulfur/zinc depletion does not affect our process of model selection via the S/Zn ratio.

The DLA system with peculiar nucleosynthetic abundances (square symbol in Fig. 2) is the only case of deviation from the reference model at almost the 3σ level. This is an example of a DLA system that does not follow the chemical evolution history described by the models considered here. However, the frequency of these systems in the DLA population is very small, as we also expect their impact to be on our methodology for calculating depletions.

5.2. Ratios of refractories to volatiles

After using the *volatile* elements to select the models of chemical evolution, we checked the ratios of *refractory to volatile* elements, X/V, predicted by these models. These ratios can be used to test the assumption that the measured abundances are uniquely determined by nucleosynthesis and depletion (Sect. 2.1). If the assumption is correct, the *measured* X/V ratios, influenced by both processes, must be lower than the *predicted* ratios, representative of the total abundance, due to the depletion of the refractories. Only in lines of sight particularly poor of dust, or for undepleted elements, should the measurements overlap with the model predictions. In any case, no measured X/V ratios should lie above the predictions: data points above the evolutionary tracks indicate either a failure in our assumption (e.g. presence of ionization effects) or the inability of the adopted model of chemical evolution to describe the intrinsic abundance ratios.

In Fig. 3, we show the X/V ratios of Mg, Si, and Fe over Zn (left panels) and S (right panels). One can see that the measurements lie below, or close to, the model predictions for all the six ratios considered. Data points above the curves, which would contradict our assumptions, are almost absent: out of a total of 189 measurements, only a couple of them lie above the models at more than the 1σ level. With these exceptions, *this comparison supports the assumption underlying our method*. It is worth recalling that in our model calculations we fixed the stellar yields, which are quite effective in changing the level of the predicted ratios. It is remarkable that the same set of stellar yields that we adopted for all of our models (François et al. 2004) is capable of reproducing the ratio of volatile elements in Fig. 2 and, at the same time, to give consistent results for all the six ratios in Fig. 3. It is encouraging that the point with the largest positive deviation from the model tracks (bottom left panel in Fig. 3) corresponds to the system at $z_{\rm abs} = 1.6265$ in QSO 0142-100, which was found to have peculiar nucleosynthetic abundances (Cooke et al. 2010). With the exception of rare cases of this type, we interpret the deviations between data and models in Fig. 3 as being caused by depletion effects.

The spread in the X/V ratios predicted by the models in Fig. 3 is larger for Mg than for either Si or Fe. This is because Mg is produced only by massive stars (core-collapse SNae), whereas Si, S, Fe, and Zn are produced in large amounts by type Ia SNae, whose progenitors are low and intermediate mass stars. As a result, the ratios Mg/Zn and Mg/S are more sensitive to variations in the star formation histories than the other ratios Si/Zn, Si/S, Fe/Zn, and Fe/S shown in the figure. This spread in the X/V ratios is included in the calculation of depletions as we explain now.

5.3. Calculation of depletions

After selecting and testing the models, we finally calculate the depletions. We proceed in two steps. We first measure $\delta_{(X;{\rm Zn})}$ and/or $\delta_{(X;{\rm S})}$ with Eq. (4). We then follow two different procedures for the DLA systems of the (Zn+S) sample, which have both measurements $\delta_{(X;{\rm Zn})}$ and $\delta_{(X;{\rm S})}$, and for those of the $\mathcal{Z}$ and $\mathcal{S}$ samples, which have only one of the two. The errors in $\delta_{(X;{\rm Zn})}$ and/or $\delta_{(X;{\rm S})}$ are calculated with the expression

$$\epsilon(\delta_{X,i}) \simeq \left(\epsilon^2_{O,i} + \epsilon^2_{\mathcal{M},i}\right)^{1/2}, \quad (9)$$

where $\epsilon_{O,i}$ is derived by propagating the measurement errors in $\log(X/V)_{O,i}$ and $\epsilon_{\mathcal{M},i}$ is the standard deviation in the predictions $\log(X/V)^{(j)}_{\mathcal{M},i}$ of the selected models calculated at the value of metallicity of the ith DLA system.

In additions to the error given in Eq. (9), the depletions are affected by a systematic error induced by the imperfect matching of individual measurements and reference model in S/Zn (Fig. 2). We can quantify this effect as follows. We define $\Delta_{\rm S/Zn} = \log({\rm S/Zn})_O - \log({\rm S/Zn})_{\mathcal{M}}$ the deviation between the observed and the predicted ratio in Fig. 2. By applying Eq. (4)

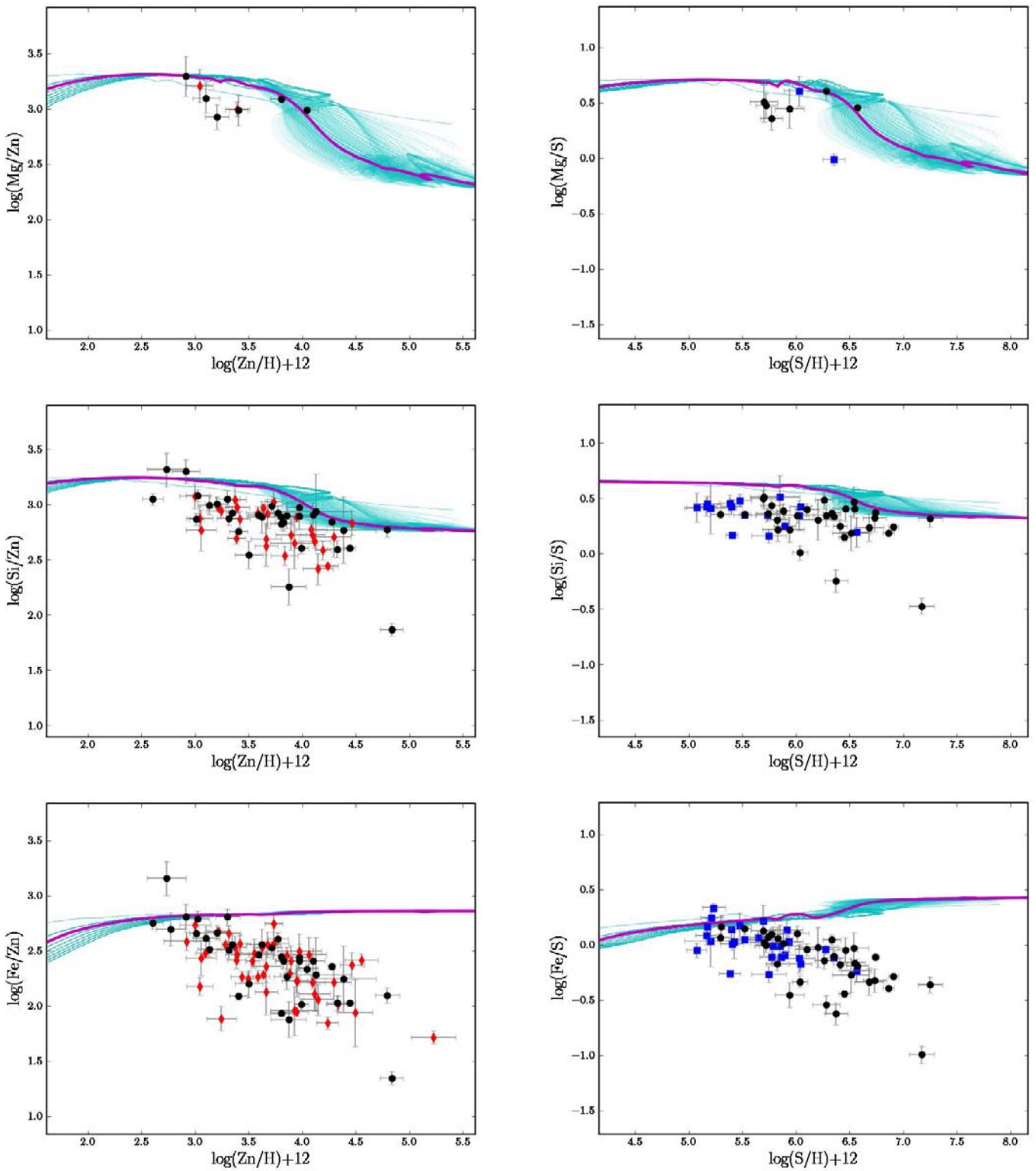

Fig. 3. Abundance ratios of the refractory elements Mg, Si, and Fe over the volatile element Zn (*left panels*) and S (*right panels*), plotted versus the absolute abundance of the volatile element. Filled symbols with error bars: measurements in DLA systems obtained from the (Zn+S) sample (black circles), the $\mathcal{Z}$ sample (red diamonds), and the $\mathcal{S}$ sample (blue squares); see Sect. 3.3. Curves: predictions obtained from the models of galactic chemical evolution selected by our procedure (same legenda as in Fig. 2, *top panel*).

twice, first with V = Zn and then with V = S, it is easy to see that the difference between the depletions calculated in the two cases is[6] $\delta_{(X;\mathrm{Zn})} - \delta_{(X;\mathrm{S})} \simeq \Delta_{\mathrm{S/Zn}}$. Therefore the deviation $\Delta_{\mathrm{S/Zn}}$ yields a systematic error $\simeq +\frac{1}{2}\Delta_{\mathrm{S/Zn}}$ on $\delta_{(X;\mathrm{Zn})}$ and $\simeq -\frac{1}{2}\Delta_{\mathrm{S/Zn}}$ on $\delta_{(X;\mathrm{S})}$. We treat these errors in two different ways in the (Zn+S) sample and in both the $\mathcal{Z}$ and $\mathcal{S}$ samples.

[6] The relation is exact if the prediction of the model of chemical evolution is such that $(\mathrm{Zn/H})_O = (\mathrm{Zn/H})_M$ at the same time in which $(\mathrm{S/H})_O = (\mathrm{S/H})_M$. This condition is generally satisfied with a good approximation.

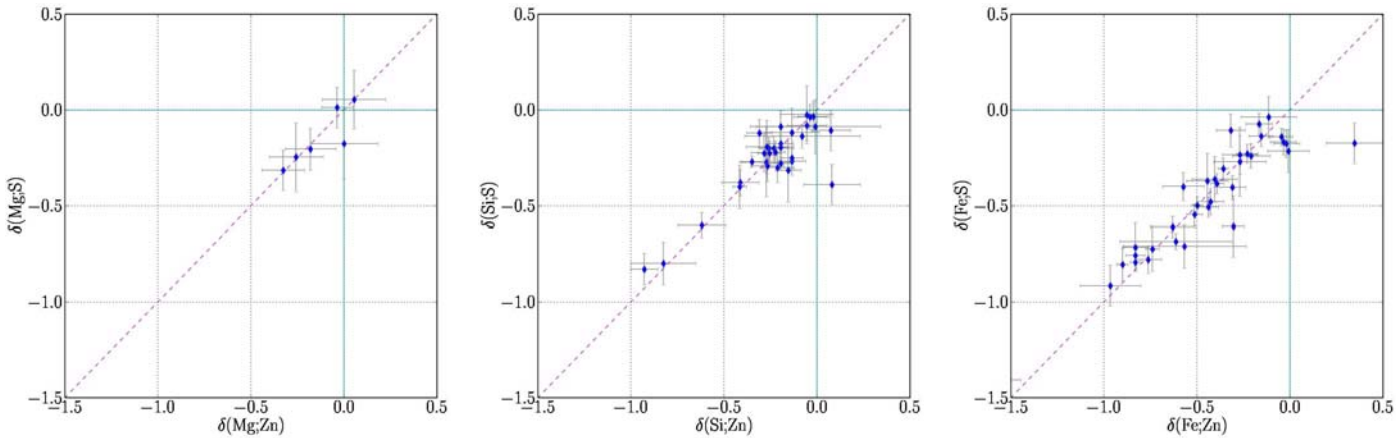

Fig. 4. Comparison of Mg, Si and depletions of the (Zn+S) sample of DLA systems obtained from different refractory/volatile abundance ratios. Abscissae: depletions obtained from ratios of refractories to Zn (see *left panels* in Fig. 3). Ordinates: depletions obtained from ratios of refractories to S (see *right panels* in Fig. 3).

Table 3. Typical values of Galactic ISM depletions and mean values of DLA depletions.

X	WH[a]	WD[a]	CD[a]	$\langle\delta_X\rangle$[b]	σ_X[b]	SEM[b]	$\delta_{X,\mathrm{med}}$[b]	n[b]	$\langle\delta_X\rangle$[c]	σ_X[c]	SEM[c]	$\delta_{X,\mathrm{med}}$[c]	n[c]
Mg	0.009	−0.390	−1.168	−0.18	0.19	0.059	−0.14	10	−0.18	0.19	0.059	−0.14	10
Si	0.095	−0.360	−1.246	−0.27	0.16	0.019	−0.23	74	−0.26	0.16	0.019	−0.23	75
Fe	−0.592	−1.106	−2.108	−0.42	0.28	0.027	−0.39	105	−0.42	0.28	0.028	−0.39	106

Notes. [(a)] Representative values of Galactic depletions in warm-halo gas (WH), warm-disk gas (WD), and cool-disk gas (CD), calculated from Eq. (10) of Jenkins (2009) with $F_* = -0.28$, 0.12, and 0.90, respectively (see Fig. 19 and Table 4 in that paper). [(b)] $\langle\delta_X\rangle$: mean value of the depletions of the DLA systems of the merged sample; σ_X: standard deviation; SEM: standard error of the mean; $\delta_{X,\mathrm{med}}$: median value of the depletions of the merged sample. [(c)] Same as in note *b*, but with the inclusion in the analysis of the DLA system at $z_{\mathrm{abs}} = 1.6265$ in QSO 0142-100.

5.3.1. The (Zn+S) sample

In this sample, we know both $\delta_{(X;\mathrm{Zn})}$ and $\delta_{(X;\mathrm{S})}$. We average these two values and derive the mean depletion $\langle\delta_X\rangle = 0.5\,[\delta_{(X;\mathrm{Zn})} + \delta_{(X;\mathrm{S})}]$. The average approximately cancels the systematic errors $\simeq+\frac{1}{2}\Delta_{\mathrm{S/Zn}}$ and $\simeq-\frac{1}{2}\Delta_{\mathrm{S/Zn}}$. Therefore *the average depletions derived for the (Zn+S) sample are almost unaffected by the mismatch between data and reference model in Fig. 2*. To assign an error to $\langle\delta_X\rangle$, we cannot use the common formulae of error propagation since $\delta_{(X;\mathrm{Zn})}$ and $\delta_{(X;\mathrm{S})}$ are not independent[7]. We instead adopt the average of the errors $\epsilon(\delta_{X,i})$ previously measured with Eq. (9).

In Fig. 4, we compare $\delta_{(X;\mathrm{S})}$ with $\delta_{(X;\mathrm{Zn})}$ the DLA systems of the (Zn+S) sample. In the three panels of the figures, we show the three refractory elements considered, i.e. Mg, Si, and Fe. One can see that the differences between $\delta_{(X;\mathrm{Zn})}$ and $\delta_{(X;\mathrm{S})}$ are generally within the errors. Systematic differences between the two are virtually cancelled by averaging $\delta_{(X;\mathrm{S})}$ and $\delta_{(X;\mathrm{Zn})}$.

5.3.2. The $\mathcal{Z}$ and $\mathcal{S}$ samples

For the DLA systems of these samples, we know either $\delta_{(X;\mathrm{Zn})}$ or $\delta_{(X;\mathrm{S})}$, but not both of them, the deviations $\Delta_{\mathrm{S/Zn}}$ of individual systems being unknown. In this case, we assume that these unknown deviations behave similarly to the deviations in the (Zn+S) sample. We calculate the standard deviation of these $\Delta_{\mathrm{S/Zn}}$ values, $\epsilon_{\mathrm{S/Zn}}$, and finally estimate the error

$$\epsilon'(\delta_{X,i}) \simeq \left[\epsilon^2(\delta_{X,i}) + \epsilon^2_{\mathrm{S/Zn}}\right]^{1/2}. \quad (10)$$

By assigning this error to the depletions of the $\mathcal{Z}$ and $\mathcal{S}$ samples, we incorporate into the error budget the effect of the mismatch between data and models in Fig. 2.

6. Discussion

We now discuss the DLA depletions derived with our method. Depletions of individual systems are shown in Figs. 5 and 6. Mean values of δ_X are listed in Table 3. The statistical properties that we present are based on the *merged sample*, i.e. the set of data obtained by merging the depletions of the (Zn+S), $\mathcal{Z}$, and $\mathcal{S}$ samples (Sect. 3.3). We do not include in the sample the DLA system with peculiar abundances at $z_{\mathrm{abs}} = 1.6265$ in QSO 0142-100; statistical results derived by including this system in the analysis are generally identical (see e.g. Table 3).

In the course of the discussion, we compare our results with typical values of Galactic ISM depletions. In performing this comparison, we must take into account that the strength of ISM depletion varies with the physical conditions of the gas. Following Savage & Sembach (1996), we consider, for each element of interest, three representative levels of depletions, corresponding to Galactic warm-halo (WH), warm-disk (WD), and cool-disk (CD) gas[8]. These reference values of Galactic ISM depletions, updated following Jenkins (2009), are listed in Table 3.

[7] Both quantities are derived using the same column density and the same model parameters for the element X.

[8] The distinction between disk and halo is based on the location (Galactic disk or halo) of the interstellar region intersected by the line of sight. Temperatures and densities in these interstellar regions tend to be inversely correlated, with typical values $T \sim 6000$ K and $n \sim 0.1$ atoms cm^{-3} in (warm) intercloud gas, and $T \sim 80$ K and $n \sim 20$ atoms cm^{-3} in (colder) diffuse clouds (Spitzer 1978).

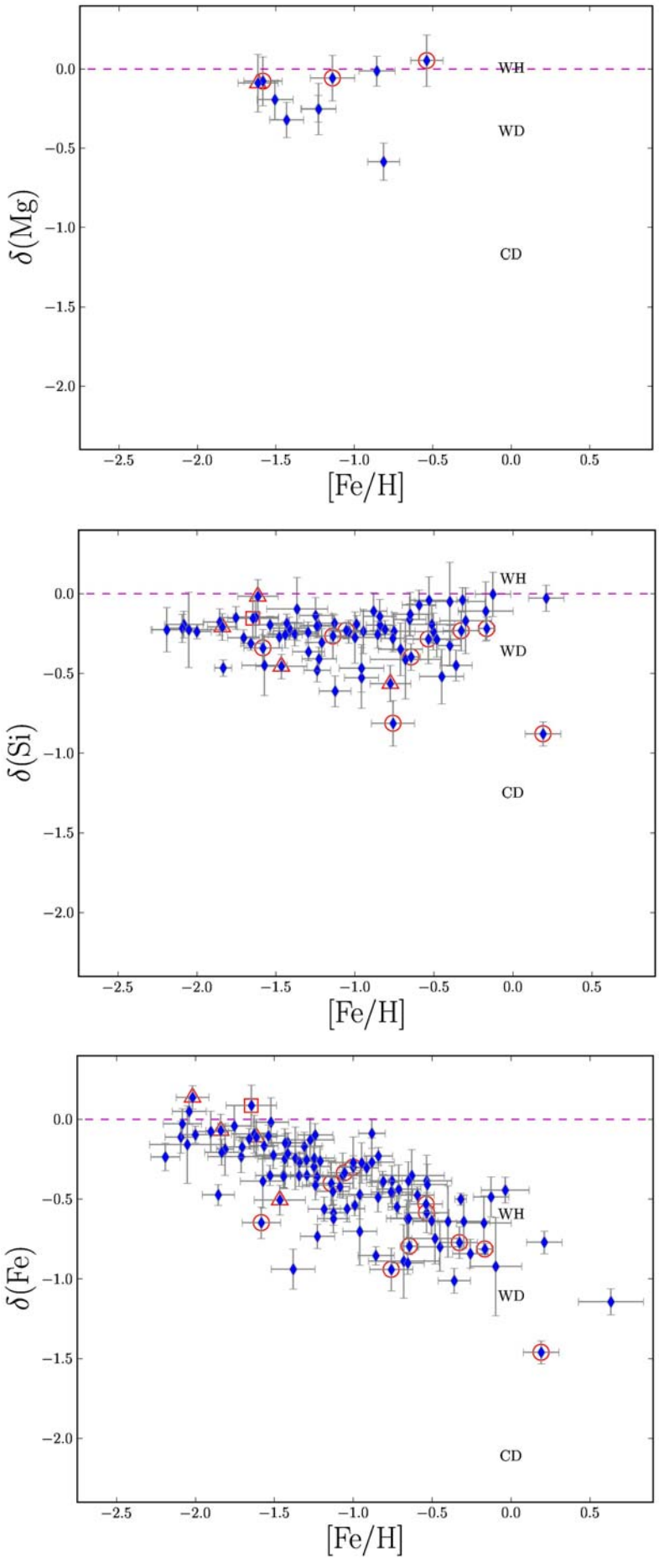

Fig. 5. Depletions of Mg, Si, and Fe in DLA systems plotted on a common scale of [Fe/H] metallicity defined in Sect. 6.2. Blue diamonds: results obtained by merging all the observational samples (Tables 4–6); molecular DLA systems are marked with red circles; proximated DLA systems with red triangles; the peculiar system at z_{abs} = 1.6265 in QSO 0142-100 is marked with a red square. The labels CD, WD, and WH indicate the typical values of Galactic ISM depletions in cool disk gas, warm disk gas, and warm halo gas, respectively (see Table 3).

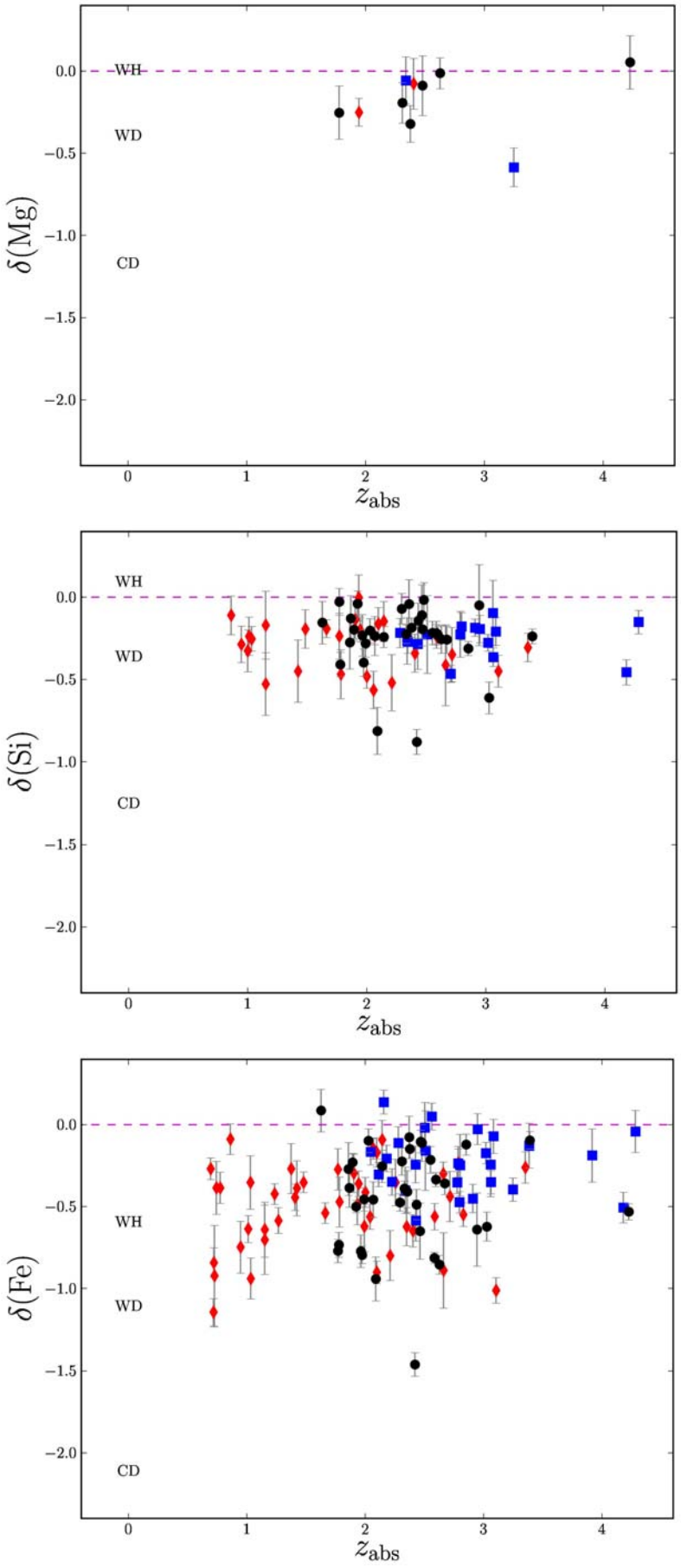

Fig. 6. Depletions of Mg, Si, and Fe versus absorption redshift in DLA systems. Symbols with error bars: data obtained from the (Zn+S) sample (black circles), the $\mathcal{Z}$ sample (red diamonds), and the $\mathcal{S}$ sample (blue squares); see Sect. 3.3. The labels CD, WD, and WH indicate the typical values of Galactic ISM depletions in cool disk gas, warm disk gas, and warm halo gas, respectively.

The depletions are negative by definition; we follow the convention of saying that a depletion is *high* (or *low*), when its absolute value $|\delta_X|$ is high (or low).

6.1. Mean values of depletion

Before studying trends between depletions and other quantities we consider the mean statistical properties shown in Table 3. The first result to point out is that the mean depletion of Mg and Si is detected, in spite of these elements being mildly depleted in the ISM and DLA depletions generally being low. The case of Si is quite strong: the mean depletion of 74 DLA systems is detected at a level of 14 times the standard error of the mean. The case of Mg is less strong: the mean depletion of ten systems is three times the error of the mean.

Silicon depletion is stronger than expected: its mean value, $\simeq -0.27$ dex, is not particularly weaker than that of iron, $\simeq -0.42$ dex. This is surprising because iron is much more depleted than silicon in the ISM, as shown in Table 3. While $\langle\delta_{\rm Fe}\rangle$ in DLA systems is consistent with the lowest Galactic ISM depletions of iron (warm *halo* gas), the mean DLA value $\langle\delta_{\rm Si}\rangle$ resembles the Galactic depletions of silicon in warm *disk* gas, which represents an ISM phase of somewhat higher level of depletion. The mean depletion of Mg is in between those of the warm halo gas and the warm disk gas.

The different behaviors of the silicon and iron depletions are also apparent from their dispersions: silicon depletions are less scattered ($\sigma_{\rm Si} = 0.16$ dex) than iron depletions ($\sigma_{\rm Fe} = 0.28$ dex). The existence of systematic differences between silicon and iron depletions is confirmed by the detailed analysis of the trend with metallicity.

6.2. Depletions versus metallicity

In Fig. 5, we plot the Mg, Si, and Fe depletions versus [Fe/H]. To establish a common scale of dust-free [Fe/H] for the systems of the (Zn+S), $\mathcal{Z}$, and $\mathcal{S}$ samples, we used the [Fe/H] value predicted by the model[9]. The depletions obtained from the different samples (Sect. 3.3) are all indicated with a blue diamond. Proximate DLA systems (Sect. 3.2) are marked with a red triangle; their depletions are generally consistent with those of intervening DLA systems.

From a simple inspection of Fig. 5, one can see that $\delta_{\rm Fe}$ increases with metallicity. To quantify the correlation between $\delta_{\rm Fe}$ and [Fe/H], we used a Spearman's rank correlation analysis. The Spearman correlation coefficient, $r_{\rm S}$, is a non-parametric measure of the statistical dependence of two variables related by any monotonic function (not just a linear function as in the case of the Pearson analysis). By applying this analysis to $\delta_{\rm Fe}$ versus [Fe/H], we find that $r_{\rm S} = -0.74$ for the merged sample of iron measurements ($n = 105$). The iron data appear to be correlated, albeit with a large scatter in $\delta_{\rm Fe}$ at each value of [Fe/H].

The iron result is not surprising because a general rise in DLA depletions with metallicity was reported in previous investigations (e.g. Ledoux et al. 2003; Vladilo 2004). For this reason, we expected to find a similar rise for silicon. However, this is not the case: by applying the Spearman analysis to $\delta_{\rm Si}$ versus [Fe/H] we find that $r_{\rm S} = +0.05$ for the merged sample of silicon measurements ($n = 74$), i.e., that *silicon depletions are not statistically correlated with metallicity*. This explains the smaller dispersion in silicon depletions seen in Table 3 ($\sigma_{\rm Si} < \sigma_{\rm Fe}$): iron varies with [Fe/H] while silicon does not.

Despite the lack of statistical correlation, a careful inspection of Fig. 5 shows that the maximum $|\delta_{\rm Si}|$ at a given [Fe/H] does increase with metallicity, put in other words *the lower envelope of silicon data decreases with [Fe/H]*. However, *the upper envelope of silicon depletions stays roughly constant* (actually showing a hint of an increase with [Fe/H]) and this explains why silicon depletion is uncorrelated with metallicity. By applying the same analysis to iron, we find a different behavior: both the minimum and the maximum $|\delta_{\rm Fe}|$ at a given [Fe/H] increase with metallicity, or in simple words *the lower and upper envelopes of iron depletions decrease with [Fe/H]*. The minimum value of $|\delta_{\rm Fe}|$ vanishes at [Fe/H] $\lesssim -1.5$.

Even if the magnesium sample is too small to derive firm conclusions, the data suggest similarities with silicon results. The Spearman analysis yields $r_{\rm S} = +0.19$ for the merged sample of $\delta_{\rm Mg}$ ($n = 10$): magnesium depletions are not statistically correlated with metallicity. The inspection of Fig. 5 suggests that the upper envelope of magnesium depletions is roughly constant, while the lower envelope seems to decrease with [Fe/H]; these results require more data to be confirmed.

In spite of the differences between iron depletions on the one hand, and silicon and magnesium depletions on the other, the comparison with Galactic ISM depletions suggests that these two sets of results have a common behavior. One can see from Fig. 5 that all the lower envelopes of $\delta_{\rm Mg}$, $\delta_{\rm Si}$, and $\delta_{\rm Fe}$, extrapolated to [Fe/H] = 0, tend to match the maximum values of Galactic ISM depletions with increasing metallicity. In contrast, all the upper envelopes of $\delta_{\rm Mg}$, $\delta_{\rm Si}$ and $\delta_{\rm Fe}$ tend to match the minimum values of Galactic ISM depletions (warm-halo gas) at [Fe/H] = 0. From these results, we tentatively propose that the depletions of different elements in DLA systems may follow a common pattern of metallicity evolution: *for a given element X, the envelope of the highest values of DLA depletions evolves with metallicity in such a way as to come close to the highest Galactic depletion of X at [Fe/H] = 0; the envelope of the lowest DLA depletions approaches the lowest Galactic depletion of X at [Fe/H] = 0*. Future investigations, based on large datasets for many chemical elements, will prove or disprove the validity of this general picture.

6.3. Depletions and physical state

The spread of Galactic depletions at [Fe/H] = 0 provides a means of interpreting the spread of DLA depletions at a given [Fe/H]. We know that the different depletion levels in the ISM reflect the variations in the physical conditions of Galactic clouds. By analogy, it is reasonable to assume that the same holds true in DLA systems, the depletions being weaker in low-density, high-temperature gas and stronger in high-density, low-temperature gas. We argue that *the spread in DLA depletions at a given [Fe/H] reflects the variation in the physical conditions of clouds embedded in galaxies with the same level of chemical enrichment*. To prove this assumption, we need to compare the depletions with measurements of physical parameters. However, we know in advance that this comparison might be biased: our measurements of depletions are probably underestimated for the lines of sight with the highest levels of depletions, owing to the possible depletion of sulfur and zinc. The highest levels of depletion are expected to occur in molecular systems that we now discuss.

[9] We converted the measured $({\rm Zn/H})_{O,i}$ ratio (or $({\rm S/H})_{O,i}$ ratio) of each system to the $({\rm Fe/H})_{\mathcal{M},i}$ ratio predicted by the reference model of chemical evolution at $({\rm Zn/H})_{\mathcal{M}} = ({\rm Zn/H})_{O,i}$ (or at $({\rm S/H})_{\mathcal{M}} = ({\rm S/H})_{O,i}$). For systems of the (Zn+S) sample, we adopted the mean value of $\log({\rm Fe/H})_{\mathcal{M},i}$ derived in this way.

6.4. Molecular DLA systems

Molecular systems are marked with a red circle in Fig. 5. As explained in Sect. 2.5.1, zinc and sulfur could be depleted in molecular systems, in which case the depletions of Mg, Si, and Fe would be underestimated by an amount equal to δ_{Zn} or δ_S (Eq. (5)). To have an approximate idea of how strong this effect might be, we estimated the maximum values expected for zinc and sulfur depletion in the most depleted regions of the Galactic ISM. Owing to the paucity of accurate measurements of sulfur depletions in high-column density Galactic lines of sight, we estimated δ_{Zn} and δ_S using Eq. (10) of Jenkins (2009) with $F_* = 1.0$. This value is representative of the highest level of Galactic depletion, generally found in molecular gas. From this indirect estimate, we find that $\delta_{Zn} \simeq -0.55$ dex and[10] $\delta_S \simeq -0.72$ dex. If we take these figures to indicate how much the depletions in molecular DLA systems may be underestimated, we can study the potential implications for our results. One can see from Fig. 5 that if we decreased the depletions of molecular systems (symbols inside red circles) by an amount in the range $\simeq -0.55/-0.72$ dex, these systems would end up more or less close to the lower envelope of DLA depletions in most cases. This would confirm our hypothesis that the spread of depletions at a given metallicity is due to variations in the physical conditions: molecular clouds would lie close to the lower envelope of maximum depletions for this reason. Therefore, the main conclusions of present discussion would be reinforced if sulfur and zinc were depleted as they are in the Galactic ISM.

6.5. Differential sulfur/zinc depletion

Six of seven molecular DLA systems lie below the reference model in Fig. 2. This systematic effect, albeit small as we discussed in Sect. 5.1.4, may indicate the existence of differential sulfur/zinc depletion if sulfur is more depleted than zinc in dust-rich, molecular lines of sight. To test this possibility, we used again the Galactic ISM as a reference. From the above-mentioned values of δ_{Zn} and δ_S along Galactic lines of sight with $F_* = 1.0$ (Jenkins 2009) we expect sulfur depletion to exceed zinc depletion by $\simeq 0.17$ dex. The deviations that we find between molecular data and reference model in Fig. 2 are typically $\simeq -0.05$ dex (-0.10 dex in two cases), consistent with an excess of sulfur over zinc depletion of that magnitude. All together, these results may represent evidence of differential sulfur/zinc depletion in DLA systems, which remains to be confirmed by future investigations.

6.6. Depletions versus absorption redshift

In Fig. 6, we plot the depletions versus the absorption redshift of the DLA systems. In this figure, the results obtained from the (Zn+S), $\mathcal{Z}$, and $\mathcal{S}$ samples are indicated with different symbols (black circles, red diamonds and blue squares, respectively). For the sake of clarity, molecular systems are not labeled in this case, even if they are present in the figure.

Figure 6 is useful to see how the Zn data (red diamonds) give a good coverage of low-redshift systems, while the S data (cyan squares) of high-redshift ones. The (Zn+S) sample for which we have measurements of both volatile elements (black circles) is limited between the redshift for detection of S II lines from ground ($z_{abs} \gtrsim 2$) and the redshift at which Zn II has mostly been detected so far ($z_{abs} \lesssim 3$). The advantage of using the $\mathcal{Z}$ and $\mathcal{S}$ samples, in addition to the (Zn+S) sample, is evident from this figure. The redshift range $2 \lesssim z_{abs} \lesssim 3$ could be used to calibrate other reference elements in future studies of DLA abundances and dust evolution.

From a simple inspection of the figure, one can see that there is no trend between depletions and redshift. The Spearman correlation analysis confirms this result, yielding $r_S = -0.05$ for δ_{Si} versus z_{abs} ($n = 74$). In the case of iron, we find that $r_S = +0.27$ for δ_{Fe} versus z_{abs} ($n = 105$). The very modest trend found for iron probably reflects the weak decrease in metallicity with redshift, found in previous investigations (e.g. Vladilo et al. 2000; Prochaska et al. 2001), combined with the trend between δ_{Fe} and metallicity discussed above. Evidently, the lack of a statistical trend between δ_{Si} and metallicity translates into the null result that we find for silicon.

The lack of dependence of depletion on absorption redshift suggests that the abundance of DLA dust and its potential effects on the extinction of background quasars should not vary significantly in the course of cosmic evolution. This result is consistent with the results from the CORALS survey, which found DLA statistics and metallicity to be largely unbiased by dust at both $z \gtrsim 1.8$ (Ellison et al. 2001; Akerman et al. 2005) and $0.7 \lesssim z \lesssim 1.6$ (Ellison et al. 2004; Ellison & Lopez 2009).

The absence of any significant trend with redshift suggests that cosmic time is not a good clock for measuring the evolution of the dust content in DLA galaxies. The metallicity is a better clock than time, at least in the case of iron. These results are in line with what we expect from studies of galactic chemical evolution: the absolute abundance of metals is a better clock of evolution than the time elapsed since the beginning of star formation.

7. Summary and conclusions

We have presented a new method for measuring elemental depletions in DLA systems. The method was developed with the aim of measuring the depletion of silicon, a basic constituent of cosmic silicates, at the early stages of chemical evolution. In addition to silicon, we applied the method to iron, for comparison with previous studies of DLA depletion, and to magnesium, an important ingredient of silicates that had not been previously investigated in studies of DLA depletions.

The method is based on the comparison of abundance ratios measured in the gas and total abundance ratios (gas plus dust) calculated from models of galactic chemical evolution. We assume that the volatile elements sulfur and zinc can be used to trace the total abundances, while the refractory elements magnesium, silicon, and iron are partly depleted from the gas into dust grains. The diagram of measured ratios S/Zn versus Zn/H is used as a dust-free diagnostic tool to constrain models of galactic chemical evolution. The models are also constrained by means of an *age test* that compares the look back time of each DLA system, inferred from its redshift, with the time elapsed after the beginning of star formation, inferred from the model.

In applying the method, we used column density measurements accumulated from the literature for 293 DLA systems. After selecting the highest quality measurements and discarding DLA systems affected by ionization, we were left with 10, 131, 66, 167, and 94 column densities of Mg II, Si II, S II, Fe II, and Zn II, respectively. These include a few measurements of S II column densities presented here.

From a set of 956 models of galactic chemical evolution, representative of a large variety of putative DLA host galaxies

[10] We adopt the most reliable of two sets of sulfur parameters, as suggested by Jenkins (2009).

(Sect. 4), we selected the model that best fits the observational diagram S/Zn versus Zn/H (Fig. 2); this model was later used as a reference to calculate the depletions. A total of 322 models, consistent with the S/Zn diagnostic tool according to the chi-square condition shown in Eq. (8), were also selected; these models were used to estimate the spread of the depletions, acknowledging that DLA systems are likely to originate in a variety of galaxies.

Our selection of galactic chemical evolution models yields conclusions consistent with previous work: most DLA systems appear to originate in a mixture of low-mass galaxies; a minority of them may originate in spiral disks. Since the population of DLA systems is probably inhomogeneous, the chi-square of the model that best fits the S/Zn versus Zn/H data, $\chi^2_\nu = 1.34$, is not particularly high. This suggests that, after all, the chemical histories of DLA systems do not differ widely, at least for the systems of the high-resolution spectroscopic sample considered here, and within the range of metallicity covered by our data ($-2 \lesssim$ [Fe/H] $\lesssim 0$).

After selecting the models using the abundances of volatile elements, we tested the ratios of *refractory to volatile* elements, X/V, predicted by these models. The calculated ratios, plotted versus V/H, should never lie below the measured ratios if our assumptions are correct. The comparison of predictions and measurements of the 6 ratios Mg/Zn, Mg/S, Si/Zn, Si/S, Fe/Zn, and Fe/S for a total of 189 data points gives a positive result in 99% of cases (Fig. 3). After this test, we calculated the depletions. With the available data, we were able to derive $\delta_{\rm Mg}$, $\delta_{\rm Si}$, and $\delta_{\rm Fe}$ for 10, 74, and 105 DLA systems, respectively. The main results that we find can be summarized as follows.

Silicon and magnesium depletions were detected, despite the mild depletion of these elements in the Galactic ISM and the low dust content of DLA systems.

The mean depletion of silicon that we find, $\langle\delta_{\rm Si}\rangle = -0.27 \pm 0.16$ dex, is almost as high as that of iron, $\langle\delta_{\rm Fe}\rangle = -0.42 \pm 0.28$ dex. The similarity between these two values is surprising since iron is much more depleted than silicon in the Galactic ISM (Table 3). The typical iron depletion in DLA systems is comparable to that of the ISM warm-*halo* gas, while the typical silicon depletion in DLA systems is comparable to that of the ISM warm-*disk* gas.

The analysis of depletions versus metallicity reveals an important difference between silicon and iron: while $\delta_{\rm Fe}$ correlates with [Fe/H] (Spearman correlation coefficient $r_{\rm S} = -0.74$), $\delta_{\rm Si}$ is not correlated ($r_{\rm S} = +0.05$). In spite of the lack of statistical correlation, the lower envelope of silicon depletions decreases with metallicity, approaching the Galactic ISM silicon depletion of cool-disk gas (Fig. 5). The upper envelope of silicon depletions plotted versus metallicity is instead roughly constant. For iron, both the lower and the upper envelope decrease with metallicity; at [Fe/H] $\lesssim -1.5$ dex, the iron depletion tends to vanish.

Magnesium depletions seem to behave more in accordance with silicon than with iron. For this element, the conclusions are tentative because of the limited size of the sample.

The behavior of iron depletions is consistent with that found in previous studies of DLA systems, which already pointed out the resemblance of $\langle\delta_{\rm Fe}\rangle$ with warm halo gas depletions, the rise in $|\delta_{\rm Fe}|$ with metallicity and the tendency of $\delta_{\rm Fe}$ to vanish at [Fe/H] $\lesssim -1.5$ dex. The different behavior that we find for silicon, and possibly magnesium, is an unexpected result of the present work.

In spite of the different behavior of Fe depletions on the one hand, and of Si and Mg depletions on the other, the comparison with Galactic ISM data suggests that all DLA depletions may follow a common pattern of evolution with metallicity: for a given element X, the envelope of the highest values of DLA depletions evolves approaching the highest value of Galactic depletion of X at [Fe/H] = 0; the envelope of the lowest values of DLA depletions approaches the lowest value of Galactic depletion of X.

The Mg, Si, and Fe depletions generally display a significant spread at a given value of [Fe/H]. By analogy with the interpretation of the spread in the Galactic depletions at constant metallicity ([Fe/H] = 0), we argue that the spread in the DLA depletions reflects the variation in the physical conditions in clouds that have attained the same level of chemical enrichment. The distribution of molecular systems, expected to have the highest levels of depletion at a given [Fe/H], is found to be broadly consistent with this hypothesis, once we take into account that their depletions might be underestimated by up to $\approx$0.5/0.7 dex due to S and Zn depletion in dust-rich gas. We find tentative evidence of differential S/Zn depletion of $\lesssim$0.1 dex in molecular systems, to be confirmed by future investigations.

No trend between depletions and redshift is detected, apart from a weak tendency for iron depletion to decrease with redshift. The lack of trends with redshift and the presence of trends with [Fe/H], at least for iron, indicates that metallicity is a better clock than cosmic time for the purpose of tracing the history of dust evolution.

The different properties of silicon and iron depletions in DLA systems have several implications. From the practical point of view, one should be careful about using silicon as a dust-free indicator of DLA metallicity in the absence of abundance measurements of volatile elements. In fact, when [Fe/H] $\lesssim -1.5$ dex, it is probably safer to use iron rather than silicon for this purpose.

From the point of view of the evolution of the dust-to-metal ratio in galaxies, the silicon results change the perspective of previous work based on iron. If a constant fraction of metals is condensed into dust in the course of chemical evolution, we expect the dust-to-metal ratio and the depletions to remain roughly constant with metallicity, apart from variations in the physical conditions of the clouds. *The depletions of silicon in DLA systems, which are approximately constant with metallicity, are in line with the expectations for a constant dust-to-metal ratio*. This is possibly also true for magnesium. At this point, the behavior which is more difficult to understand is that of iron. The decrease in $\delta_{\rm Fe}$ at the lowest DLA metallicities, already known from previous studies, suggests the existence of some mechanism that inhibits the production of iron-rich dust at the early stages of chemical evolution ([Fe/H] $\lesssim -1.5$ dex).

Taken together, our results indicate that the behavior of DLA depletions is more complex than expected and may vary from element to element. To study the variation of the total dust-to-metal ratio, we should first investigate the evolution of the depletions of all the cosmically abundant elements. In general, measuring depletions for a variety of elements in DLA systems is essential to constrain models of dust production in the course of chemical evolution (Dwek 1998; Calura et al. 2008; Zhukovska et al. 2008). We hope that our methodology and results may open new possibilities for future studies of this kind and, in particular, for studies of cosmic silicates at high redshift.

Acknowledgements. We thank Cristina Chiappini and Francesco Calura for helpful discussions at the early stages of preparation of this work; C.A. thanks Miriam Centurión for her support in the analysis of UVES spectra; J.Y. thanks the financial support from the National Science Foundation of China No. 10573028, the Key Project No. 10833005, the Group Innovation Project No. 10821302, 973 program No. 2007CB815402, and the Knowledge Innovation Program of the Chinese Academy of Sciences No. Y090761009. We thank an anonymous referee for her/his helpful comments and suggestions.

References

Akerman, C. L., Ellison, S. L., Pettini, M., & Steidel, C. C. 2005, A&A, 440, 499
Alibés, A., Labay, J., & Canal, R. 2001, A&A, 370, 1103
Asplund, M., Grevesse, N., & Sauval, A. J. 2005, ASP Conf. Ser., 336, 25
Bevington, P. R., & Robinson, D. K. 1992, Data Reduction and Error Analysis for the Physical Sciences (McGraw-Hill, Inc.)
Bradamante, F., Matteucci, F., & D'Ercole, A. 1998, A&A, 337, 338
Calura, F., Matteucci, F., & Vladilo, G. 2003, MNRAS, 340, 59
Calura, F., Pipino, A., & Matteucci, F. 2008, A&A, 479, 669
Centurión, M., Bonifacio, P., Molaro, P., & Vladilo, G. 2000, ApJ, 536, 540
Centurión, M., Molaro, P., Vladilo, G., et al. 2003, A&A, 403, 55
Cescutti, G., Matteucci, F., François, P., & Chiappini, C. 2007, A&A, 462, 943
Cescutti, G., Matteucci, F., McWilliam, A., & Chiappini, C. 2009, A&A, 505, 605
Chang, R. X., Hou, J. L., Shu, C. G., & Fu, C. Q. 1999, A&AS, 141, 491
Chiappini, C., Matteucci, M. F., & Gratton, R. G. 1997, ApJ, 477, 765
Chiappini, C., Matteucci, M. F., & Romano, D. 2001, ApJ, 554, 1044
Chiappini, C., Hirschi, R., Meynet, G., et al. 2006, A&A, 449, L27
Cooke, R., Pettini, M., Steidel, C. C., et al. 2010, MNRAS, 409, 679
Dessauges-Zavadsky, M., Calura, F., Prochaska, J. X., D'Odorico, S., & Matteucci, F. 2004, A&A, 416, 79
Dessauges-Zavadsky, M., Prochaska, J. X., D'Odorico, S., Calura, F., & Matteucci, F. 2006, A&A, 445, 93
Draine, K. 2003, ARA&A, 41, 241
Dunkley, J., Komatsu, E., Nolta, M. R., et al. 2009, ApJS, 180, 306
Dwek, E. 1998, ApJ, 501, 643
Ellison, S. L., & Lopez, S. 2009, MNRAS, 397, 467
Ellison, S. L., Yan, L., Hook, I. M., et al. 2001, A&A, 379, 393
Ellison, S. L., Churchill, C. W., Rix, S. A., & Pettini, M. 2004, ApJ, 615, 118
Ellison, S. L., Prochaska, J. X., Hennawi, J., et al. 2010, MNRAS, 406, 1435
Field, G. B. 1974, ApJ, 187, 543
Fontana, A., & Ballester, P. 1995, The Messenger, 80, 37
François, P., Matteucci, F., Cayrel, R., et al. 2004, A&A, 421, 613
Frank, S., & Péroux, C. 2010, MNRAS, 406, 2235
Fynbo, J. P. U., Noterdaeme, P., Christensen, L., et al. 2011, MNRAS, in press [arXiv:1011.5312]
Gry, C., York, D. G., & Vidal-Madjar, A. 1985, 296, 593
Haehnelt, M. G., Steinmetz, M., & Rauch, M. 1998, ApJ, 495, 647
Henning, T. 2010, ARA&A, 48, 21
Jenkins, E. B. 2009, ApJ, 700, 1299
Jiang, P., Ge, J., Prochaska, J. X., et al. 2010, ApJ, 720, 328
Jimenez, R., Bowen, D. V., & Matteucci, F. 1999, ApJ, 514, L83
Jorgenson, R. A., Wolfe, A. M., Prochaska, J. X., et al. 2006, ApJ, 646, 730
Junkkarinen, V. T., Cohen, R. D., Beaver, E. A., et al. 2004, ApJ, 614, 658
Kulkarni, V. P., York, D. G., Vladilo, G., & Welty, D. E. 2007, ApJ, 663, L81
Kulkarni, V. P., Torres, L., Som, D., et al. 2011, ApJ, in press
Le Brun, V., Bergeron, J., Boissé, P., & Deharveng, J. M. 1997, A&A, 321, 733
Ledoux, C., Petitjean, P., & Srianand, R. 2003, MNRAS, 346, 209
Lodders, K. 2003, ApJ, 591, 1220
Lu, L., Sargent, W. L. W., Barlow, T. A., Churchill, C. W., & Vogt, S. S. 1996, ApJS, 107, 475
Matteucci, M. F., & François, P. 1989, MNRAS, 239, 885
Matteucci, F., Molaro, P., & Vladilo, G. 1997, A&A, 321, 45
Møller, P., Warren, S. J., & Fynbo, J. U. 1998, A&A, 330, 19
Morton, D. C. 2003, ApJS, 149, 205
Murphy, M. T., & Liske, J. 2004, MNRAS, 354, L31
Noterdaeme, P., Petitjean, P., Srianand, R., Ledoux, C., & Le Petit, F. 2007, A&A, 469, 425
Noterdaeme, P., Ledoux, C., Petitjean, P., & Srianand, R. 2008, A&A, 481, 327
Péroux, C., Dessauges-Zavadsky, M., D'Odorico, S., Kim, T.-S., & McMahon, R. G. 2007, MNRAS, 382, 177
Péroux, C., Bouché, N., Kulkarni, V. P., York, D. G., & Vladilo, G. 2011, MNRAS, 410, 2237
Pettini, M., Smith, L. J., Hunstead, R. W., & King, D. L. 1994, ApJ, 426, 79
Pettini, M., Smith, L. J., King, D. L., & Hunstead, R. W. 1997, ApJ, 486, 665
Prantzos, N., & Boissier, S. 2000a, MNRAS, 313, 338
Prantzos, N., & Boissier, S. 2000b, MNRAS, 315, 82
Prochaska, J. X., & Wolfe, A. M. 1997, ApJ, 487, 73
Prochaska, J. X., Gawiser, E., & Wolfe, A. M. 2001, ApJ, 552, 99
Prochaska, J. X., Howk, J. C., O'Meara, J. M., et al. 2002, ApJ, 571, 693
Prochaska, J. X., O'Meara, J. M., Herbert-Fort, S., et al. 2006, ApJ, 648, L97
Rix, S. A., Pettini, M., Steidel, C. C., et al. 2007, ApJ, 670, 15
Salpeter, E. E. 1955, ApJ, 121, 161
Savage, B. D., & Sembach, K. R. 1991, 379, 245
Savage, B. D., & Sembach, K. R. 1996, ARA&A, 34, 279
Scalo, J. M. 1986, Fundam. Cosmic Phys., 11, 1
Scappini, F., Cecchi-Pestellini, C., Smith, H., Klemperer, W., & Dalgarno, A. 2003, MNRAS, 341, 657
Sofia, U. J., Gordon, K. D., Clayton, G. C., et al. 2006, ApJ, 636, 753
Spitzer, L. Jr. 1978, in Physical Processes in the Interstellar Medium (New York: Wiley & Sons)
Srianand, R., Gupta, N., Petitjean, P., Noterdaeme, P., & Saikia, D. J. 2008a, MNRAS, 391, L69
Srianand, R., Noterdaeme, P., Ledoux, C., & Petitjean, P. 2008b, A&A, 482, L39
Ueda, Y., Mitsuda, K., & Murakami, H. 2005, ApJ, 620, 274
Vladilo, G. 2002, A&A, 391, 407
Vladilo, G. 2004, A&A, 421, 479
Vladilo, G., Bonifacio, P., Centurión, M., & Molaro, P. 2000, ApJ, 543, 24
Vladilo, G., Centurión, M., Bonifacio, P., & Howk, J. C. 2001, ApJ, 557, 1007
Vladilo, G., Centurión, M., Levshakov, S. A., et al. 2006, A&A, 454, 151
Vladilo, G., Prochaska, J. X., & Wolfe, A. M. 2008, A&A, 478, 701
Wang, J., Hall, P. B., Ge, J., Li, A., & Schneider, D. P. 2004, ApJ, 609, 589
Weatherley, S. J., Warren, S. J., Møller, P., et al. 2005, MNRAS, 358, 985
Welty, D. E., Lauroesch, J. T., Blades, J. C., Hobbs, L. M., & York, D. G. 2001, ApJ, 554, L75
Wolfe, A. M., Turnshek, D. A., Smith, H. E., & Cohen, R. D. 1986, ApJS, 61, 249
Wolfe, A. M., Lanzetta, K. M., Foltz, C. B., & Chaffee, F. H. 1995, ApJ, 454, 698
Wolfe, A. M., Gawiser, E., & Prochaska, J. X. 2005, ARA&A, 43, 861
Yin, J., Magrini, L., Matteucci, F., et al. 2010, A&A, 520, 55
Zhukovska, S., Gail, H.-P., & Trieloff, M. 2008, A&A, 453, 480

Pages 19 to 23 are available in the electronic edition of the journal at http://www.aanda.org

Table 4. The Zn+S sample of DLA systems selected as explained in Sect. 3.

Systems used to constrain the models of galactic chemical evolution										
QSO	z_{qso}	z_{abs}	log N(H I)	log N(Zn II)	log N(S II)	r(Zn II)[a]	r(S II)[a]	r(Mg II)[a]	r(Si II)[a]	r(Fe II)[a]
0000−263	4.120	3.3901	21.41 ± 0.08	12.01 ± 0.05	14.70 ± 0.03	20c	16d	—	20c	20c
0010−0012	2.165	2.0250	20.95 ± 0.10	12.25 ± 0.05	14.96 ± 0.05	23d	25d	—	25d	23d
0058−2914	3.070	2.6711	21.10 ± 0.10	12.23 ± 0.05	14.92 ± 0.03	23d	25d	—	25d	23d
0100+130	2.690	2.3090	21.37 ± 0.08	12.47 ± 0.10	15.09 ± 0.06	24a	24a	24a	—	24a
0102−1902	3.025	2.3693	21.00 ± 0.08	11.77 ± 0.11	14.30 ± 0.04	23d	25d	—	—	23d
0201+365	2.912	2.4620	20.38 ± 0.04	12.76 ± 0.30	15.29 ± 0.02	16e	22j	—	22j	22j
0216+080	2.992	2.2931	20.50 ± 0.10	12.47 ± 0.05	15.04 ± 0.02	26e	31P	—	16d	31P
0347−383	3.230	3.0250	20.73 ± 0.05	12.23 ± 0.12	14.76 ± 0.05	23d	25d	—	23d	22e
0405−443	3.020	2.5505	21.13 ± 0.10	12.44 ± 0.05	14.82 ± 0.06	23e	23e	—	23e	23e
0528−2505	2.779	2.1410	20.95 ± 0.05	12.29 ± 0.03	14.83 ± 0.04	26e	23a	—	23a	23a
0812+32	2.701	2.6260	21.35 ± 0.10	13.15 ± 0.02	15.63 ± 0.08	27h	27h	27h	27h	27h
0841+129	2.4934[c]	2.3745	21.00 ± 0.10	12.20 ± 0.05	14.77 ± 0.03	23a	23a	26a	27b	23a
0841+129	2.4934[c]	2.4764	20.78 ± 0.08	11.69 ± 0.10	14.48 ± 0.10	26a	26a	26a	26a	26a
0953+5230	1.875	1.7680	20.10 ± 0.10	12.89 ± 0.05	15.35 ± 0.05	26k	26k	—	26k	26k
1116+4118A	2.971	2.9422	20.28 ± 0.05	12.40 ± 0.33	15.01 ± 0.10	27j	27j	—	27j	27j
1210+1731	2.543	1.8918	20.63 ± 0.08	12.40 ± 0.05	14.96 ± 0.03	27b	27b	—	27b	27b
1223+178	2.936	2.4661	21.40 ± 0.10	12.42 ± 0.05	15.14 ± 0.04	23d	25d	—	25d	23d
1331+170	2.100	1.7764	21.14 ± 0.08	12.54 ± 0.02	15.08 ± 0.11	24a	24a	24a	24a	24a
2138−4427	3.170	2.8510	20.98 ± 0.05	11.99 ± 0.05	14.50 ± 0.02	23d	25d	—	25d	23d
2206−199A	2.559	1.9200	20.68 ± 0.03	12.95 ± 0.02	15.42 ± 0.02	21i	31P	—	ww1	31P
2222−0946	2.927	2.3540	20.65 ± 0.05	12.75 ± 0.10	15.19 ± 0.13	31A	31A	—	31A	31A
2230+025	2.147	1.8642	20.83 ± 0.05	12.80 ± 0.11	15.29 ± 0.10	26a	26a	—	26a	26a
2231−0015	3.015	2.0662	20.59 ± 0.08	12.30 ± 0.05	15.10 ± 0.15	24a	24a	—	24a	24a
2243−6031	3.010	2.3300	20.67 ± 0.02	12.47 ± 0.02	15.02 ± 0.03	26e	22f[b]	—	22f	22f
2314−409	2.448	1.8573	20.90 ± 0.10	12.52 ± 0.10	15.10 ± 0.15	21c	21c	—	21c	21c
2318−1107	2.960	1.9890	20.68 ± 0.05	12.50 ± 0.06	15.09 ± 0.04	27f	27f	—	27f	27f
2343+1232	2.549	2.4313	20.40 ± 0.07	12.25 ± 0.10	14.66 ± 0.05	27f	27f	—	27f	27f
Molecular DLA systems[d] with $f(H_2) > 10^{-4.5}$										
QSO	z_{qso}	z_{abs}	log N(H I)	log N(Zn II)	log N(S II)	r(Zn II)[a]	r(S II)[a]	r(Mg II)[a]	r(Si II)[a]	r(Fe II)[a]
0013−004	2.087	1.9731	20.83 ± 0.05	12.82 ± 0.04	15.28 ± 0.02	22h	22h	—	22h	22h
0405−443	3.020	2.5950	21.09 ± 0.10	12.68 ± 0.02	15.19 ± 0.05	23e	23e	—	23e	23e
0551−3637	2.317	1.9615	20.70 ± 0.08	13.02 ± 0.05	15.38 ± 0.11	22d	22d	—	22d	22d
0918+1636	3.073	2.5832	20.96 ± 0.05	13.40 ± 0.02	15.82 ± 0.02	31C	31C	—	31C	31C
1439+1117	2.583	2.4184	20.10 ± 0.10	12.93 ± 0.04	15.27 ± 0.06	28d	28d	—	28d	28d
1443+2724	4.420	4.2240	20.95 ± 0.10	12.99 ± 0.03	15.52 ± 0.02	28c	26f	26f	—	26f
1444+014	2.210	2.0870	20.25 ± 0.07	12.12 ± 0.15	14.62 ± 0.08	23d	23d	—	23d	23d
DLA system with peculiar nucleosynthetic abundances[e]										
0142−100A[e]	2.730	1.6265	20.70 ± 0.10	11.43 ± 0.15	14.53 ± 0.10	30a	30a	—	30a	30a

Notes. [a] Reference code for the column density of the ion. Codes are specified in Table 7. [b] Value of log N(S II) corrected for unseen components by the authors. [c] Emission redshift from Ellison et al. (2010). [d] Values of $f(H_2)$ taken from Noterdaeme et al. (2008), Srianand et al. (2008b), and Fynbo et al. (2011). [e] See Cooke et al. (2010). The quasar is also known as UM 673A.

Table 5. The $\mathcal{Z}$ sample: DLA systems with measurements of Zn II, but not S II, column densities.

QSO	z_{qso}	z_{abs}	log N(H I)	log N(Zn II)	r(Zn II)[a]	r(Mg II)[a]	r(Si II)[a]	r(Fe II)[a]
0149+33	2.431	2.1410	20.50 ± 0.10	11.50 ± 0.10	ww1	—	ww1	ww1
0203−0910	1.580	1.0280	21.18 ± 0.14	13.15 ± 0.15	29d	—	—	29d
0216+080	2.992	1.7688	20.30 ± 0.10	11.97 ± 0.07	26e	—	16d	16d
0225+0054	2.970	2.7140	21.00 ± 0.10	12.89 ± 0.10	26c	—	26c	26c
0256+0110	1.348	0.7250	20.70 ± 0.16	13.19 ± 0.04	26j	—	—	26j
0302−223	1.400	1.0095	20.36 ± 0.11	12.45 ± 0.04	20e	—	20e	20e
0354−2724	2.823	1.4051	20.18 ± 0.15	12.73 ± 0.03	27e	—	—	27e
0438−436	2.863	2.3474	20.78 ± 0.10	12.72 ± 0.03	25a	—	—	25a
0454+039	1.343	0.8597	20.69 ± 0.06	12.42 ± 0.06	28a	—	20e	20e
0458−02	2.286	2.0400	21.70 ± 0.10	13.13 ± 0.02	ww1	—	—	19e
0515−4414	1.710	1.1510	20.45 ± 0.10	12.11 ± 0.04	20b	—	20b	20b
0812+32	2.701	2.0668	21.00 ± 0.10	12.21 ± 0.02	27h	—	27h	27h
0933+733	2.525	1.4790	21.62 ± 0.09	12.71 ± 0.02	25e	—	—	25e
0935+417	1.936	1.3726	20.52 ± 0.10	12.25 ± 0.10	15b	—	—	15b
0948+433	1.892	1.2330	21.62 ± 0.06	13.15 ± 0.02	25e	—	—	25e
1010+0003	1.399	1.2651	21.52 ± 0.07	13.01 ± 0.02	28a	—	—	26g
1013+0035	4.405	3.1040	21.10 ± 0.10	13.33 ± 0.02	27h	—	27h	27h
1055−301	2.523	1.9035	21.54 ± 0.10	12.91 ± 0.03	25a	—	25a	25a
1104−1805	2.319	1.6616	20.85 ± 0.01	12.48 ± 0.02	19b	—	19b	19b
1107+0048	1.391	0.7410	21.00 ± 0.05	13.06 ± 0.15	26j	—	—	26j
1116+4118A	2.971	2.6617	20.48 ± 0.10	12.40 ± 0.20	27j	—	27j	27j
1117−1329	3.960	3.3511	20.84 ± 0.08	12.25 ± 0.06	22g	—	22g	22g
1137+3907	1.023	0.7190	21.10 ± 0.10	13.43 ± 0.05	26g	—	—	26g
1157+0128	1.9920[c]	1.9436	21.60 ± 0.10	12.99 ± 0.05	27b	27b	27b	27b
1209+0919	3.297	2.5841	21.40 ± 0.10	12.98 ± 0.05	27h	—	27h	27h
1215+33	2.606	1.9990	20.95 ± 0.07	12.33 ± 0.05	ww1	—	19e	ww1
1225+0035	1.226	0.7731	21.38 ± 0.12	13.23 ± 0.07	28a	—	—	26g
1230−101	2.394	1.9314	20.48 ± 0.10	12.94 ± 0.05	25a	—	25a	25a
1249−0233	2.120	1.7810	21.45 ± 0.10	13.11 ± 0.10	26c	—	26c	26c
1253−0228	4.010	2.7830	21.85 ± 0.20	12.77 ± 0.07	23g	—	—	23g
1323−0021	1.388	0.7160	20.21 ± 0.20	13.43 ± 0.05	26i	—	—	26i
1328+307	0.846	0.6922	21.25 ± 0.02	12.53 ± 0.03	28j	—	—	28j
1351+318	1.326	1.1491	20.23 ± 0.10	12.52 ± 0.13	19d	—	19d	19d
1354+258	2.030	1.4200	21.54 ± 0.06	12.59 ± 0.13	19d	—	19d	19d
1426+6039	3.170	2.8268	20.30 ± 0.04	12.18 ± 0.04	27h	—	—	27h
1451+1223	3.246	2.2550	20.30 ± 0.15	11.85 ± 0.11	23b	—	—	23b
1501+0019	1.930	1.4832	20.85 ± 0.13	12.93 ± 0.06	26g	—	26g	—
1727+5302	1.444	0.9449	21.16 ± 0.14	13.27 ± 0.05	24c	—	24c	24c
1727+5302	1.444	1.0311	21.41 ± 0.13	12.65 ± 0.05	24c	—	24c	24c
1733+5533	1.072	0.9984	20.70 ± 0.04	12.80 ± 0.06	28a	—	26g	—
1850+40	2.120	1.9900	21.40 ± 0.10	13.30 ± 0.10	18g	—	—	18g
2059−0528	2.540	2.2100	20.80 ± 0.10	12.90 ± 0.10	26c	—	26c	26c
2228−3954	2.210	2.0950	21.20 ± 0.10	12.50 ± 0.05	28c	—	—	28c
2340−00	2.0829[c]	2.0545	20.80 ± 0.10	12.60 ± 0.08	27h	—	27h	—
2359−0216	2.810	2.0950	20.65 ± 0.10	12.60 ± 0.03	19e	—	ww1	ww1
Molecular systems[b] with $f(H_2) > 10^{-4.5}$								
0027−1836	2.560	2.4020	21.75 ± 0.10	12.79 ± 0.07	28b	28b	28b	28b
0642−5038	3.090	2.6590	20.95 ± 0.08	12.57 ± 0.03	28c	—	—	28c

Notes. [a] Reference code for the column density of the ion. Codes are specified in Table 7; [b] values of $f(H_2)$ taken from Noterdaeme et al. (2008); [c] emission redshift from Ellison et al. (2010).

Table 6. The $\mathcal{S}$ sample: DLA systems with measurements of S II, but not Zn II, column densities.

QSO	z_{qso}	z_{abs}	log N(H I)	log N(S II)	r(S II)[a]	r(Mg II)[a]	r(Si II)[a]	r(Fe II)[a]
0112+029	2.819	2.4230	20.90 ± 0.10	14.83 ± 0.08	23d	—	—	23d
0135−273	3.210	2.8000	21.00 ± 0.10	14.78 ± 0.14	23d	—	—	23d
0201+1120	3.610	3.3848	21.30 ± 0.10	15.21 ± 0.11	ww1	—	—	ww1
0242−2917	3.270	2.5600	20.90 ± 0.10	14.11 ± 0.04	28c	—	—	28c
0254−4025	2.280	2.0460	20.45 ± 0.08	14.10 ± 0.04	28c	—	—	28c
0255+00	3.9936[c]	3.9146	21.30 ± 0.05	14.72 ± 0.02	ww1	—	—	ww1
0300−3152	2.370	2.1790	20.80 ± 0.10	14.20 ± 0.04	28c	—	—	28c
0336−0142	3.197	3.0621	21.10 ± 0.10	14.99 ± 0.02	22j	—	26e	22j
0425−5214	2.2639[c]	2.2240	20.30 ± 0.10	14.07 ± 0.04	28c	—	—	28c
0741+4741	3.220	3.0174	20.48 ± 0.10	14.00 ± 0.02	ww1	—	22j	22j
0900+4215	3.294	3.2458	20.30 ± 0.10	14.65 ± 0.02	27h	—	—	27h
0957+33	4.2088[c]	4.1798	20.65 ± 0.15	14.39 ± 0.06	ww1	—	ww1	ww1
1021+3001	3.120	2.9490	20.70 ± 0.10	13.87 ± 0.07	27h	27h	27h	27h
1036−2257	3.130	2.7770	20.93 ± 0.05	14.79 ± 0.02	23g	—	—	23g
1132+2243	2.880	2.7830	21.00 ± 0.07	14.07 ± 0.06	23g	—	23g	23g
1220−1800	2.160	2.1130	20.12 ± 0.07	14.39 ± 0.03	28c	—	—	28c
1337+1121	2.919	2.7957	20.95 ± 0.10	14.33 ± 0.02	27h	—	27h	27h
1354−1046	3.0112[c]	2.5010	20.44 ± 0.05	14.13 ± 0.10	28c	—	—	28c
1435+5359	2.636	2.3427	21.05 ± 0.10	14.78 ± 0.05	27c	—	27c	—
1558−0031	2.830	2.7026	20.67 ± 0.05	14.07 ± 0.02	27c	—	27c	—
2059−360	3.0974	2.5073	20.29 ± 0.07	13.49 ± 0.23	25d	—	25d	23d
2059−360	3.0974[c]	3.0830	20.98 ± 0.08	14.38 ± 0.05	25d	—	25d	20d
2222−3939	2.1832[c]	2.1540	20.85 ± 0.10	14.08 ± 0.03	28c	—	—	28c
2241+1352	4.440	4.2820	21.10 ± 0.10	14.58 ± 0.03	23g	—	23g	23g
2332−0924	3.330	3.0572	20.50 ± 0.07	14.34 ± 0.18	25d	—	23g	23d
2342+3417	2.917	2.9082	21.15 ± 0.10	15.19 ± 0.02	27h	—	27h	27h
2348−147	2.940	2.2790	20.59 ± 0.08	13.75 ± 0.06	26a	—	26a	26a
Molecular systems[b] with $f(H_2) > 10^{-4.5}$								
QSO	z_{abs}	log N(H I)	log N(S II)	r(S II)[a]	r(Mg II)[a]	r(Si II)[a]	r(Fe II)[a]	
1232+0815	2.56700	2.3377	20.80 ± 0.10	14.83 ± 0.10	23a	20h	23a	23a
2348−0108	3.01000	2.4272	20.50 ± 0.10	15.06 ± 0.10	27g	—	27g	27g

Notes. [(a)] Reference code for the column density of the ion. Codes are specified in Table 7; [(b)] values of $f(H_2)$ taken from Noterdaeme et al. (2008); [(c)] emission redshift from Ellison et al. (2010).

Table 7. Reference codes for Tables 1, 4–6.

Code	Reference
15b	Meyer, D. M., Lanzetta, K. M., & Wolfe, A. M. 1995, ApJ, 451, L13
16d	Lu, L., Sargent, W. L. W., Barlow, T. A., Churchill, C. W., & Vogt, S. S. 1996, ApJS, 107, 475
16e	Prochaska, J. X., & Wolfe, A. M. 1996, ApJ, 470, 403
18g	Prochaska, J. X., & Wolfe, A. M. 1998, ApJ, 507, 113
19b	Lopez, S., Reimers, D., Rauch, M., Sargent, W. L. W., & Smette, A. 1999, ApJ, 513, 598
19d	Pettini, M., Ellison, S. L., Steidel, C. C., & Bowen, D. V. 1999, ApJ, 510, 576
19e	Prochaska, J. X., & Wolfe, A. M. 1999, ApJS, 121, 369
20b	de la Varga, A., Reimers, D., Tytler, D., Barlow, T., & Burles, S. 2000, A&A, 363, 69
20c	Molaro, P., Bonifacio, P., Centurion, M., et al. 2000, ApJ, 541, 54
20d	Petitjean, P., Srianand, R., & Ledoux, C. 2000, A&A, 364, L26
20e	Pettini, M., Ellison, S., Steidel, C. C., Shapley, A. E., & Bowen, D. V. 2000, ApJ, 532, 65
20h	Srianand, R., Petitjean, P., & Ledoux, C. 2000, Nature, 408, 931
21c	Ellison, S. L., & Lopez, S. 2001, A&A, 380, 117
21i	Ellison, S. L., Ryan, S. G., & Prochaska, J. X. 2001, MNRAS, 326, 62
22d	Ledoux, C., Srianand, R., & Petitjean, P. 2002, A&A, 392, 781
22e	Levshakov, S. A., Dessauges-Zavadsky, M., D'Odorico, S., & Molaro, P. 2002, ApJ, 565, 696
22f	Lopez, S., Reimers, D., D'Odorico, S., & Prochaska, J. X. 2002, A&A, 385, 778
22g	Peroux, C., Petitjean, P., Aracil, B., & Srianand, R. 2002, NewA, 7, 577
22h	Petitjean, P., Srianand, R., & Ledoux, C. 2002, MNRAS, 332, 383
22j	Prochaska, J. X., Henry, R. B. C., O'Meara, J. M., et al. 2002, PASP, 114, 933
23a	Centurion, M., Molaro, P., Vladilo, G., et al. 2003, A&A, 403, 55
23b	Dessauges-Zavadsky, M., Peroux, C., Kim, T.-S., D'Odorico, S., & McMahon, R. G. 2003, MNRAS, 35, 447
23d	Ledoux, C., Petitjean, P., & Srianand, R. 2003, MNRAS, 346, 209
23e	Lopez, S., & Ellison, S. L. 2003, A&A, 403, 573
23g	Prochaska, J. X., Gawiser, E., Wolfe, A. M., Cooke, J., & Gelino, D. 2003, ApJS, 147, 227
24a	Dessauges-Zavadsky, M., Calura, F., Prochaska, J. X., D'Odorico, S., & Matteucci, F. 2004, A&A, 416, 79
24c	Khare, P., Kulkarni, V. P., Lauroesch, J. T., et al. 2004, ApJ, 616, 86
25a	Akerman, C. L., Ellison, S. L., Pettini, M., & Steidel, C. C. 2005, A&A, 440, 499
25d	Srianand, R., Petitjean, P., Ledoux, C., Ferland, G., & Shaw, G. 2005, MNRAS, 362, 549
25e	Rao, S. M., Prochaska, J. X., Howk, J. C., & Wolfe, A. M. 2005, AJ, 129, 9
26a	Dessauges-Zavadsky, M., Prochaska, J. X., D'Odorico, S., Calura, F., & Matteucci, F. 2006, A&A, 445, 93
26c	Herbert-Fort, S., Prochaska, J. X., Dessauges-Zavadsky, M., et al. 2006, PASP, 118, 1077
26e	Ledoux, C., Petitjean, P., Fynbo, J. P. U., Moller, P., & Srianand, R. 2006, A&A, 457, 71
26f	Ledoux, C., Petitjean, P., & Srianand, R. 2006, ApJ, 640, L25
26g	Meiring, J. D., Kulkarni, V. P., Khare, P., et al. 2006, MNRAS, 370, 43
26i	Peroux, C., Kulkarni, V. P., Meiring, J., et al. 2006, A&A, 450, 53
26j	Peroux, C., Meiring, J. D., Kulkarni, V. P., et al. MNRAS, 372, 369
26k	Prochaska, J. X., O'Meara, J. M., Herbert-Fort, S., et al. 2006, ApJ, 648, L97
27b	Dessauges-Zavadsky, M., Calura, F., Prochaska, J. X., D'Odorico, S., & Matteucci, F. 2007, A&A, 470, 431
27c	Henry, R. B. C., & Prochaska, J. X. 2007, PASP, 119, 962
27e	Meiring, J. D., Lauroesch, J. T., Kulkarni, V. P., et al. 2007, MNRAS, 376, 557
27f	Noterdaeme, P., Ledoux, C., Petitjean, P., et al. 2007, A&A, 474, 393
27g	Noterdaeme, P., Petitjean, P., Srianand, R., Ledoux, C., & Le Petit, F. 2007, A&A, 469, 425
27h	Prochaska, J. X., Wolfe, A. M., Howk, J. C., et al. 2007, ApJS, 171, 29
27j	Ellison, S. L., Hennawi, J. F., Martin, C. L., & Sommer-Larsen, J. 2007, MNRAS, 378, 801
28a	Nestor, D. B., Pettini, M., Hewett, P. C., Rao, S., & Wild, V. 2008, MNRAS, 390, 1670
28b	Noterdaeme, P. 2008, Ph.D. Thesis
28c	Noterdaeme, P., Ledoux, C., Petitjean, P., & Srianand, R. 2008, A&A, 481, 327
28d	Noterdaeme, P., Petitjean, P., Ledoux, C., Srianand, R., & Ivanchik, A. 2008, A&A, 491, 397
28j	Wolfe, A. M., Jorgenson, R. A., Robishaw, T., Heiles, C., & Prochaska, J. X. 2008, Nature, 455, 638
29d	Monier, E. M., Turnshek, D. A., Rao, S. M., & Weyant, A. 2009, AJ, 138, 1609
30a	Cooke, R., Pettini, M., Steidel, C. C., et al. 2010, MNRAS, 409, 679
31A	Fynbo, J. P. U., Laursen, P., Ledoux, C., et al. 2010, MNRAS, in press
31C	Fynbo, J. P. U., Noterdaeme, P., Christensen, L., et al. 2010 [arXiv:1011.5312]
31P	This work
ww1	Prochaska, J. X., DLAs Keck database at http://www.ucolick.org/~xavier

Table 8. Evolutionary tracks of the reference model of galactic chemical evolution used to estimate DLA depletions.

t (Gyr)	12+log(Mg/H)	12+log(Si/H)	12+log(S/H)	12+log(Fe/H)	12+log(Zn/H)
0.10100E−01	0.35906E+01	0.37941E+01	0.30710E+01	0.30242E+01	0.82463E+00
0.15100E−01	0.43462E+01	0.44181E+01	0.37487E+01	0.37146E+01	0.12876E+01
0.20100E−01	0.46964E+01	0.47222E+01	0.40644E+01	0.40868E+01	0.15388E+01
0.25100E−01	0.49187E+01	0.49160E+01	0.42614E+01	0.43311E+01	0.17088E+01
0.30100E−01	0.50778E+01	0.50565E+01	0.44037E+01	0.45060E+01	0.18359E+01
0.35100E−01	0.51960E+01	0.51642E+01	0.45127E+01	0.46324E+01	0.19355E+01
0.40100E−01	0.52919E+01	0.52522E+01	0.46016E+01	0.47348E+01	0.20179E+01
0.45100E−01	0.53720E+01	0.53263E+01	0.46766E+01	0.48202E+01	0.20881E+01
0.50100E−01	0.54407E+01	0.53904E+01	0.47412E+01	0.48934E+01	0.21492E+01
0.55100E−01	0.55006E+01	0.54466E+01	0.47981E+01	0.49572E+01	0.22034E+01
...	...	...	...	...	...

Notes. This model is that of a dwarf galaxy with parameters $M_{\rm infall} = 1 \times 10^9\ M_\odot$, $\epsilon = 0.4$ Gyr^{-1}, and normal wind with $\lambda_w = 3.5$ Gyr^{-1}. More details on the model can be found in Sect. 4. The criteria followed to select this particular model are explained in Sect. 5.1.3. Abundance ratios are by number and are expressed in a logarithmic scale with log(H) ≡ 12. The complete table is available in electronic form at the CDS.